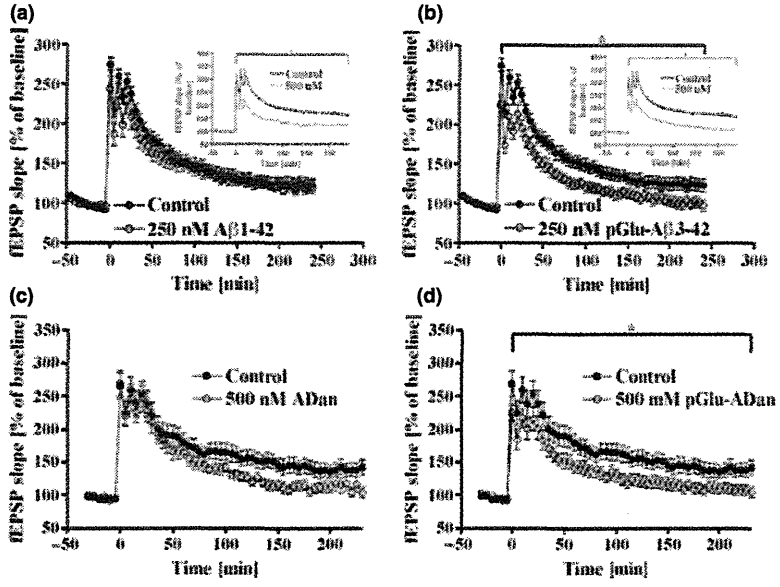

Fig. 6 Influence of Aβ1-42 (a), pGlu-Aβ3-42 (b), ADan (c) and pGlu-ADan (d) LTP in hippocampal slices from mice. In contrast to Aβ38 and Aβ40, Aβ1-42 and pGlu-Aβ3-42 significantly impaired LTP at a concentration of 500 nM (Insets). At lower concentration (250 nM) only N-terminal pGlu-modified Aβ42 (b) decreased synaptic response. Likewise, pGlu-modified ADan (d) impaired LTP. A tendency to impairment of LTP was also observed with ADan (c), however, the effect did not reach statistical significance. For experimental details, see Methods (control: $n \geq 17$, peptide: $n \geq 12$, $^*p \leq 0.05$ ANOVA with repeated measures).

(Shirotani *et al.* 2002). The cells were transfected with various APP constructs that favor the formation of either of the three Aβ species. The APP-NL construct contains the Swedish and London mutation. As a result, the cells mainly secrete Aβ1-40/42. The APP-NLE additionally includes a deletion of the first two amino acids of Aβ. Furthermore, in APP-NLQ amino acid 3 of Aβ is substituted by glutamine (E599Q). These modifications of APP result in the secretion of Aβ3-40/42 and pGlu-Aβ3-40/42, respectively (Figure S5). Application of the conditioned media from APP-NLE and APP-NL (containing primarily Aβ3-40 and Aβ1-40, respectively) to hippocampal slices revealed a non-significant influence on the synaptic function (Fig. 7). The tendency in reduction of LTP is most likely caused by the Aβ3-42 and Aβ1-42 peptides generated by the transfected cells and released to the culture medium. In accordance with the previous findings, a treatment of slices with conditioned medium containing pGlu-Aβ3-40/42, which was obtained from APP-NLQ transfected cells, caused a significant disruption of LTP. A further analysis of the oligomeric state of the Aβ peptides within the media using size exclusion chromatography in combination with ELISA quantification revealed most of the Aβ being monomer/dimer. Only in case of APP-NLQ transfected cells, the medium contained soluble higher oligomeric Aβ eluting close to the void volume (Fig. 7b), illustrating the rapid oligomerization of pGlu-modified Aβ in cell-based conditions.

Discussion

In Alzheimer's disease accumulating evidence attributes cognitive deficits to so-called 'soluble oligomers' of amyloid β peptide (Lambert *et al.* 1998; Walsh and Selkoe 2004; Cleary *et al.* 2005; Walsh *et al.* 2005; Townsend *et al.* 2006). Notably, the appearance of Aβ oligomers rather correlates with the development of AD than the total amyloid burden in the brain (Shankar *et al.* 2008). Sub-micromolar concentrations of Aβ oligomers were frequently shown to have detrimental effects on brain cells, for example, impairment of synaptic function and induction of neuronal cell death whereby, the disruption of LTP is an early aspect reflecting the collapse of glutamatergic dendritic spines (Hsieh *et al.* 2006; Rönicke *et al.* 2011).

Aβ42 species which precede deposition of Aβ40 (Iwatsubo *et al.* 1994; Lemere *et al.* 1996), have been shown to potently affect the neuronal physiology (Murakami *et al.* 2003; Irie *et al.* 2005). A truncation of the C-terminus (Jarrett *et al.* 1993) leads to much slower aggregation and oligomer formation, which correlates with lower potential to affect long-term potentiation. Although there is compelling evidence for an oligomer-induced neurotoxicity, the actual composition of the oligomers exerting toxicity apparently varies and is still matter of further investigations. Species, which have been suggested to be particularly toxic range from dimers (Shankar *et al.* 2008) to trimers (Cleary *et al.* 2005) up to, for instance, larger diffusible globulomers (Lesne *et al.* 2006; Nimmrich *et al.* 2008). However, it is not unlikely that different Aβ oligomers co-exist *in vivo*. These might share common structural features, which mediate the toxic potential (Kayed *et al.* 2003).

Here, we show that an N-terminal pGlu-modification might account for rapid oligomer formation and oligomer-induced neurophysiological changes. In previous investigations, it has been shown that N-terminally truncated and modified forms of Aβ40 and Aβ42, in particular pGlu-Aβ3-x, show a decreased solubility and a significantly enhanced

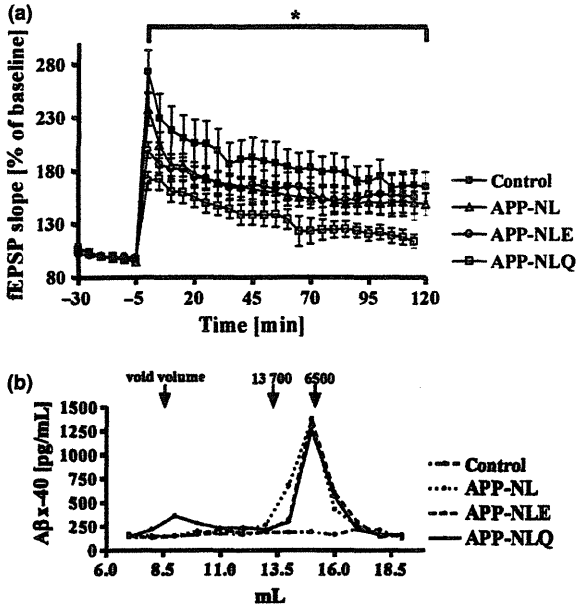

Fig. 7 Influence of conditioned media from transfected HEK293 cells on LTP (a) and oligomeric state of Aβ in these media (b). The conditioned media were collected after transient expression of the APP-forms APP-NL, APP-NLE and APP-NLQ, which results in secretion of Aβ1-x, Aβ3-x or pGlu-Aβ3-x into the medium (see Figure S5). Within the media, Aβ40 peptides represent the dominant form. The total Aβ concentration in the media did not differ substantially after transfection, slight differences where adjusted by dilution. (a) In accordance with the previous investigations, we observed a significant impairment of LTP with conditioned medium containing pGlu-Aβ3-x peptides (control: $n \geq 10$, peptides: $n \geq 12$, $^*p \leq 0.05$ ANOVA with repeated measures). (b) Two hundred and fifty microliters of conditioned media were fractionated by size exclusion chromatography (Superdex 75, 10/300) and concentration of Aβ in the fractions was analyzed by ELISA. Only the conditioned medium from APP-NLQ expressing cells contained detectable amounts of soluble oligomeric Aβ, which elutes close to the void volume of the column. Thus, pGlu-Aβ formation coincides with enforced formation of oligomeric Aβ in the cell-based system. Arrows with numbers indicate the elution of standard proteins (masses in Da).

propensity to aggregation (He and Barrow 1999; Schilling *et al.* 2006; D'Arrigo *et al.* 2009; Schlenzig *et al.* 2009). Our present study shows that N-terminal truncation and modification causes an accelerated aggregation into ThT-fluorescent conglomerates of Aβ37/38/40/42 and ADan in general (Fig. 1). In accordance with numerous studies from the literature, we found the highest propensity of Aβ42 to form such aggregates. Interestingly, those Aβ species which form fibrils most rapidly, give rise to instant formation of oligomers, as analyzed using PICUP chemistry and electron microscopy.

The PICUP pattern, however, differ between Aβ42 and its C-terminally truncated counterparts Aβ38 and Aβ40. While with Aβ42 species, that is, Aβ1-42 and pGlu-Aβ3-42, a prominent formation of trimers and tetramers can be concluded, the bands observed with pGlu-Aβ3-40 and pGlu-Aβ3-38 are less clearly defined and might correspond to trimers. In contrast, the PICUP and electron microscopic analysis of Aβ1-40 and Aβ1-38 did not provide a clear hint to rapid oligomer formation upon dissolution. Although the actual structure of the instantly formed oligomers from pGlu-Aβ3-40 and pGlu-Aβ3-38 appears to bear differences compared with Aβ42, the aggregates potently affect the neuronal physiology as investigated by hippocampal LTP. In accordance with the observation of oligomers in PICUP analysis, we only detected an influence of species on LTP, when a presence of oligomeric forms was observed in PICUP and when an increased hydrophobicity was concluded from the effect of the peptides on ANS fluorescence intensity. Moreover, the analysis of conditioned media from cultured cells clearly suggests that the effect is not limited to synthetic Aβ species but is intrinsically mediated by the N-terminal truncation and modification, even at lower concentrations and physiological mixtures of different Aβ forms as produced by transfected cells.

The presented data demonstrate clearly a direct influence of the N-terminal pGlu-modification of Aβ peptides on the velocity to form oligomers and their polar nature, which then apparently translates into an accelerated formation of larger aggregates with fibrillar characteristics. A typical property of these fibrils is that those share a bundled arrangement, potentially mediated by hydrophobic lateral interactions. The N-terminal truncation and pGlu-modification of Aβ leads to a loss of N-terminal charge, which has been suggested to result in a significant increase of hydrophobicity (D'Arrigo *et al.* 2009; Schlenzig *et al.* 2009). Interestingly, recent studies involving different amyloid species point to a crucial impact of oligomeric surface hydrophobicity on the neurotoxic potential (Bolognesi *et al.* 2010; Campioni *et al.* 2010). Likewise, the N-terminus-mediated oligomer formation of Aβ might provoke forms, which very potently mediate interaction with hydrophobic cell surfaces and receptors. Hence, the pGlu-modification basically increases hydrophobicity, which might be the main determinant for the pathogenic potency. Such a hypothesis is supported by our investigations of ADan, which provided similar results with regard to the influence of the pGlu-residue at the N-terminus. Again, the modification leads to an increase of the aggregation velocity, it impacts the fibrillar appearance and the oligomeric pattern in solution or conditioned medium, which in turn, massively affects the LTP as shown here for the first time.

Several lines of evidence suggest that the accumulation of N-terminally truncated and modified forms of Aβ correlate with the progression or severity of disease. For instance, presence of water-soluble pGlu-Aβ3-42 was linked to AD patients (Piccini *et al.* 2005) and pGlu-modified Aβ-species accumulated during progression of disease in human AD

deposits, in contrast to Aβ1-42 (Guntert *et al.* 2006). In addition, the inherited forms of AD caused by mutations in the presenilin genes are accompanied by very early and dominant appearance of truncated and modified forms of Aβ (Russo *et al.* 2000; Miravalle *et al.* 2005). Finally, attenuation of pGlu-Aβ formation has shown therapeutic efficacy in mouse models of AD (Schilling *et al.* 2008). Direct overexpression of pGlu-Aβ in a mouse model is accompanied by a severe injured phenotype and high lethality (Alexandru *et al.* 2011). The results presented here provide further evidence for a specific pathogenic role of pGlu-modified amyloid peptides, which links the accumulation of such species in AD, FBD and FDD to a potential pathophysiological function. Our observations might thus provide also implications for current treatment strategies, which primarily focus on reduction of total Aβ or more subtle of the Aβ1-42 formation and toxicity.

Acknowledgement

The work was supported by the Federal Ministry of Education and Science of Germany (BMBF), grant no. 0315223 to probiodrug AG (HUD).

Supporting information

Additional supporting information may be found in the online version of this article:

Figure S1. Aggregation kinetics of Aβx-40 (a) and Aβx-42 (b) at pH 8.0 and 37°C, monitored by ThT-fluorescence.

Figure S2. SDS–PAGE analysis of Aβ40, Aβ38 and Aβ37 following photo-induced cross-linking of unmodified peptides (PICUP), including Aβ3-x.

Figure S3. Influence of Aβx-40 on fluorescence intensity of ANS.

Figure S4. Influence of freshly dissolved Aβ3-40 on long-term potentiation (LTP) in acute hippocampal slices from mice.

Figure S5. Analysis of Aβ forms in conditioned media of HEK293 cells after transient transfection with APP constructs APP-NL, APP-NLE and APP-NLQ.

As a service to our authors and readers, this journal provides supporting information supplied by the authors. Such materials are peer reviewed and may be re-organised for online delivery, but are not copy-edited or typeset. Technical support issues arising from supporting information (other than missing files) should be addressed to the authors.

References

Alexandru A., Jagla W., Graubner S. *et al.* (2011) Neurotoxicity and lethal phenotype of pE3-Aβ expression in a transgenic mouse model – pE3-Aβ formation and neuronal loss in TBA2.1 mice. *J. Neurosci.* **31**, 12790–12801.

Bitan G., Kirkitadze M. D., Lomakin A., Vollers S. S., Benedek G. B. and Teplow D. B. (2003) Amyloid beta-protein (Abeta) assembly: Abeta 40 and Abeta 42 oligomerize through distinct pathways. *Proc. Natl Acad. Sci. USA* **100**, 330–335.

Bolognesi B., Kumita J. R., Barros T. P., Esbjorner E. K., Luheshi L. M., Crowther D. C., Wilson M. R., Dobson C. M., Favrin G. and Yerbury J. J. (2010) ANS binding reveals common features of cytotoxic amyloid species. *ACS Chem. Biol.* **5**, 735–740.

Campioni S., Mannini B., Zampagni M. *et al.* (2010) A causative link between the structure of aberrant protein oligomers and their toxicity. *Nat. Chem. Biol.* **6**, 140–147.

Cardamone M. and Puri N. K. (1992) Spectrofluorimetric assessment of the surface hydrophobicity of proteins. *Biochem. J.*, **282**(Pt 2), 589–593.

Cleary J. P., Walsh D. M., Hofmeister J. J., Shankar G. M., Kuskowski M. A., Selkoe D. J. and Ashe K. H. (2005) Natural oligomers of the amyloid-beta protein specifically disrupt cognitive function. *Nat. Neurosci.* **8**, 79–84.

Cynis H., Scheel E., Saido T. C., Schilling S. and Demuth H. U. (2008) Amyloidogenic processing of amyloid precursor protein: evidence of a pivotal role of glutaminyl cyclase in generation of pyroglutamate-modified amyloid-beta. *Biochemistry* **47**, 7405–7413.

D'Arrigo C., Tabaton M. and Perico A. (2009) N-terminal truncated pyroglutamyl beta amyloid peptide Abetapy3-42 shows a faster aggregation kinetics than the full-length Abeta1-42. *Biopolymers* **91**, 861–873.

Ellis K. J. and Morrison J. F. (1982) Buffers of constant ionic strength for studying pH-dependent processes. *Methods Enzymol.* **87**, 405–426.

Ghiso J., Revesz T., Holton J. *et al.* (2001) Chromosome 13 dementia syndromes as models of neurodegeneration. *Amyloid* **8**, 277–284.

Güntert A., Dobeli H. and Bohrmann B. (2006) High sensitivity analysis of amyloid-beta peptide composition in amyloid deposits from human and PS2APP mouse brain. *Neuroscience* **143**, 461–475.

He W. and Barrow C. J. (1999) The A beta 3-pyroglutamyl and 11-pyroglutamyl peptides found in senile plaque have greater beta-sheet forming and aggregation propensities in vitro than full-length A beta. *Biochemistry* **38**, 10871–10877.

Hsieh H., Boehm J., Sato C., Iwatsubo T., Tomita T., Sisodia S. and Malinow R. (2006) AMPAR removal underlies Abeta-induced synaptic depression and dendritic spine loss. *Neuron* **52**, 831–843.

Irie K., Murakami K., Masuda Y., Morimoto A., Ohigashi H., Ohashi R., Takegoshi K., Nagao M., Shimizu T. and Shirasawa T. (2005) Structure of beta-amyloid fibrils and its relevance to their neurotoxicity: implications for the pathogenesis of Alzheimer's disease. *J. Biosci. Bioeng.* **99**, 437–447.

Iwatsubo T., Odaka A., Suzuki N., Mizusawa H., Nukina N. and Ihara Y. (1994) Visualization of A beta 42(43) and A beta 40 in senile plaques with end-specific A beta monoclonals: evidence that an initially deposited species is A beta 42(43). *Neuron*, **13**, 45–53.

Jarrett J. T., Berger E. P. and Lansbury Jr P. T. (1993) The carboxy terminus of the beta amyloid protein is critical for the seeding of amyloid formation: implications for the pathogenesis of Alzheimer's disease. *Biochemistry* **32**, 4693–4697.

Kayed R., Head E., Thompson J. L., McIntire T. M., Milton S. C., Cotman C. W. and Glabe C. G. (2003) Common structure of soluble amyloid oligomers implies common mechanism of pathogenesis. *Science* **300**, 486–489.

Klafki H. W., Wiltfang J. and Staufenbiel M. (1996) Electrophoretic separation of betaA4 peptides (1-40) and (1-42). *Anal. Biochem.* **237**, 24–29.

Lambert M. P., Barlow A. K., Chromy B. A. *et al.* (1998) Diffusible, nonfibrillar ligands derived from Abeta1-42 are potent central nervous system neurotoxins. *Proc. Natl Acad. Sci. USA* **95**, 6448–6453.

Lemere C. A., Blusztajn J. K., Yamaguchi H., Wisniewski T., Saido T. C. and Selkoe D. J. (1996) Sequence of deposition of heterogeneous amyloid beta-peptides and APO E in Down syndrome: implications for initial events in amyloid plaque formation. *Neurobiol. Dis.* **3**, 16–32.

Lesne S., Koh M. T., Kotilinek L., Kayed R., Glabe C. G., Yang A., Gallagher M. and Ashe K. H. (2006) A specific amyloid-beta protein assembly in the brain impairs memory. *Nature* **440**, 352–357.

Miravalle L., Calero M., Takao M., Roher A. E., Ghetti B. and Vidal R. (2005) Amino-terminally truncated Abeta peptide species are the main component of cotton wool plaques. *Biochemistry* **44**, 10810–10821.

Murakami K., Irie K., Morimoto A., Ohigashi H., Shindo M., Nagao M., Shimizu T. and Shirasawa T. (2003) Neurotoxicity and physicochemical properties of Abeta mutant peptides from cerebral amyloid angiopathy: implication for the pathogenesis of cerebral amyloid angiopathy and Alzheimer's disease. *J. Biol. Chem.* **278**, 46179–46187.

Nimmrich V., Grimm C., Draguhn A., Barghorn S., Lehmann A., Schoemaker H., Hillen H., Gross G., Ebert U. and Bruehl C. (2008) Amyloid beta oligomers (A beta(1-42) globulomer) suppress spontaneous synaptic activity by inhibition of P/Q-type calcium currents. *J. Neurosci.* **28**, 788–797.

Piccini A., Russo C., Gliozzi A. *et al.* (2005) {beta}-amyloid is different in normal aging and in Alzheimer disease. *J. Biol. Chem.* **280**, 34186–34192.

Rönicke R., Schroder U. H., Bohm K. and Reymann K. G. (2009) The Na+/H+ exchanger modulates long-term potentiation in rat hippocampal slices. *Naunyn. Schmiedebergs. Arch. Pharmacol.* **379**, 233–239.

Rönicke R., Mikhaylova M., Ronicke S., Meinhardt J., Schroder U. H., Fandrich M., Reiser G., Kreutz M. R. and Reymann K. G. (2011) Early neuronal dysfunction by amyloid beta oligomers depends on activation of NR2B-containing NMDA receptors. *Neurobiol. Aging* **32**, 2219–2228.

Russo C., Schettini G., Saido T. C., Hulette C., Lippa C., Lannfelt L., Ghetti B., Gambetti P., Tabaton M. and Teller J. K. (2000) Presenilin-1 mutations in Alzheimer's disease. *Nature* **405**, 531–532.

Schilling S., Lauber T., Schaupp M., Manhart S., Scheel E., Bohm G. and Demuth H. U. (2006) On the seeding and oligomerization of pGlu-amyloid peptides (in vitro). *Biochemistry* **45**, 12393–12399.

Schilling S., Zeitschel U., Hoffmann T. *et al.* (2008) Glutaminyl cyclase inhibition attenuates pyroglutamate Abeta and Alzheimer's disease-like pathology. *Nat. Med.* **14**, 1106–1111.

Schlenzig D., Manhart S., Cinar Y., Kleinschmidt M., Hause G., Willbold D., Funke S. A., Schilling S. and Demuth H. U. (2009) Pyroglutamate formation influences solubility and amyloidogenicity of amyloid peptides. *Biochemistry* **48**, 7072–7078.

Shankar G. M., Li S., Mehta T. H. *et al.* (2008) Amyloid-beta protein dimers isolated directly from Alzheimer's brains impair synaptic plasticity and memory. *Nat. Med.* **14**, 837–842.

Shirotani K., Tsubuki S., Lee H. J., Maruyama K. and Saido T. C. (2002) Generation of amyloid beta peptide with pyroglutamate at position 3 in primary cortical neurons. *Neurosci. Lett.* **327**, 25–28.

Townsend M., Shankar G. M., Mehta T., Walsh D. M. and Selkoe D. J. (2006) Effects of secreted oligomers of amyloid beta-protein on hippocampal synaptic plasticity: a potent role for trimers. *J. Physiol.* **572**, 477–492.

Walsh D. M. and Selkoe D. J. (2004) Deciphering the molecular basis of memory failure in Alzheimer's disease. *Neuron* **44**, 181–193.

Walsh D. M., Hartley D. M., Condron M. M., Selkoe D. J. and Teplow D. B. (2001) In vitro studies of amyloid beta-protein fibril assembly and toxicity provide clues to the aetiology of Flemish variant (Ala692–>Gly) Alzheimer's disease. *Biochem. J.* **355**, 869–877.

Walsh D. M., Townsend M., Podlisny M. B., Shankar G. M., Fadeeva J. V., Agnaf O. E., Hartley D. M. and Selkoe D. J. (2005) Certain inhibitors of synthetic amyloid beta-peptide (Abeta) fibrillogenesis block oligomerization of natural Abeta and thereby rescue long-term potentiation. *J. Neurosci.* **25**, 2455–2462.

THE JOURNAL OF BIOLOGICAL CHEMISTRY VOL. 287, NO. 31, pp. 25834–25843, July 27, 2012

Contribution of the γ-Secretase Subunits to the Formation of Catalytic Pore of Presenilin 1 Protein*

Received for publication, December 30, 2011, and in revised form, June 5, 2012 Published, JBC Papers in Press, June 11, 2012, DOI 10.1074/jbc.M111.336347

Koji Takeo[‡1], **Naoto Watanabe**[‡1], **Taisuke Tomita**[‡§2], **and Takeshi Iwatsubo**[‡§¶]

From the [‡]*Department of Neuropathology and Neuroscience, Graduate School of Pharmaceutical Sciences and the* [¶]*Department of Neuropathology, Graduate School of Medicine, The University of Tokyo, Tokyo 113-0033 and the* [§]*Core Research for Evolutional Science and Technology, Japan Science and Technology Corporation, Tokyo 113-0033, Japan*

Background: γ-Secretase, which is composed of presenilin and three subunits, is an intramembrane-cleaving protease related to Alzheimer disease.
Results: Water accessibility of the catalytic pore of presenilin was decreased during assembly of active γ-secretase.
Conclusion: Binding of the subunits allosterically contributes to the formation of catalytic pore.
Significance: The γ-secretase subunits modulate the structure of presenilin.

γ-Secretase is an intramembrane-cleaving protease related to the etiology of Alzheimer disease. γ-Secretase is a membrane protein complex composed of presenilin (PS) and three indispensable subunits: nicastrin, Aph-1, and Pen-2. PS functions as a protease subunit forming a hydrophilic catalytic pore structure within the lipid bilayer. However, it remains unclear how other subunits are involved in the pore formation. Here, we show that the hydrophilic pore adopted with an open conformation has already been formed by PS within the immature γ-secretase complex. The binding of the subunits induces the close proximity between transmembrane domains facing the catalytic pore. We propose a model in which the γ-secretase subunits restrict the arrangement of the transmembrane domains of PS during the formation of the functional structure of the catalytic pore.

γ-Secretase is the responsible enzyme for generation of amyloid-β peptide (Aβ),[3] which is the major component of senile plaques in the brains of patients with Alzheimer disease (1). Genetic studies revealed that numerous point mutations in *presenilin* (*PSEN*) genes are linked to familial Alzheimer disease. These mutations affect the γ-secretase activity in a way that increases the generation of Aβ ending at the 42nd residue (*i.e.* Aβ42), which is the most aggregable species and predominantly deposited in the brains of Alzheimer disease patients (2, 3). Genetic and chemical biology approaches revealed that PS, a nine membrane-spanning protein, is the catalytic subunit of the γ-secretase (1, 2). Thus, PS/γ-secretase is an attractive molecular target for the development of Alzheimer disease therapeutics. γ-Secretase belongs to the family of intramembrane-cleaving protease that cleaves transmembrane domains (TMDs) of a number of membrane proteins. Recent structural analyses revealed the atomic molecular structures of rhomboid and site-2 protease, which are the other members of the intramembrane-cleaving proteases. Both proteases harbor an intramembranous chamber in which the catalytic residues are located. This atypical structure enables water to have access to the catalytic center within the lipid bilayer (4). However, γ-secretase is a membrane protein complex composed of PS and three other subunits: nicastrin (Nct), Aph-1, and Pen-2 (5, 6). PS interacts with the Nct-Aph-1 subcomplex and Pen-2 in the endoplasmic reticulum. PS then undergoes endoproteolysis to generate N- and C-terminal fragments (NTF and CTF, respectively). Thus, very limited information regarding the structure of the γ-secretase is available so far as the active form of the enzyme is composed of five transmembrane protein subunits with 19 TMDs. To overcome this issue, we have employed chemical biology approaches, *i.e.* substituted cysteine accessibility method (SCAM) and chemical cross-linking experiments coupled with application of γ-secretase inhibitors (7–10). Using these approaches, we and others have shown that PS, a catalytic subunit of the γ-secretase, forms a hydrophilic structure within the lipid bilayer (7, 11). However, it still remains unknown whether the other γ-secretase subunits contribute to the formation of the catalytic pore structure in PS during the γ-secretase assembly. Here, we analyzed the structural differences of the pore of PS1 mutants that are unable to bind with the subunits and found that the binding of the subunits regulated the structure of the catalytic site.

* This work was supported in part by grants-in-aid for young scientists (S) (to T. T.) from the Japan Society for the Promotion of Science (JSPS), by the Targeted Proteins Research Program of the Japan Science and Technology Corporation (JST) (to T. T. and T. I.), by Core Research for Evolutional Science and Technology of JST (to T. T. and T. I.), and by the Strategic Research Program for Brain Sciences "Analysis of the molecular basis of brain aging and degeneration due to failure in metabolic homeostasis and environmental stress" by the Ministry of Education, Culture, Sports, Science and Technology, Japan.
[1] Research fellows of the JSPS.
[2] To whom correspondence should be addressed: Dept. of Neuropathology and Neuroscience, Graduate School of Pharmaceutical Sciences, The University of Tokyo, 7-3-1 Hongo, Bunkyo-ku, Tokyo 113-0033, Japan. Tel.: 81-3-5841-4868; Fax: 81-3-5841-4708; E-mail: taisuke@mol.f.u-tokyo.ac.jp.
[3] The abbreviations used are: Aβ, amyloid-β peptide; CTF, carboxyl-terminal fragment; NTF, amino-terminal fragment; DKO, PS1/PS2 double knockout fibroblasts; Nct, nicastrin; mt, mutant; MTSEA, *N*-biotinaminoethyl methanethiosulfonate; PS, presenilin; SCAM, substituted cysteine accessibility method; TMD, transmembrane domain; NEM, *N*-ethylmaleimide; M2M, 1,2-ethanediyl bismethanethiosulfonate; Cu-Phe, copperphenanthroline; CHAPSO, 3-[(3-cholamidopropyl)dimethylammonio]-2-hydroxy-1-propanesulfonate.

EXPERIMENTAL PROCEDURES

Plasmid Construction, Cell Culture, Transfection, Retroviral Infection, and Baculoviral Infection—For expression in mammalian cells, cDNAs encoding human PS1 mutants were inserted into pMXs-puro (7–10, 12). cDNAs encoding mutant PS1 were generated by long PCR-based QuikChange™ strategy (Stratagene). For the expression of γ-secretase subunits in Sf9 cells, PS1 mutants and Aph-1aL-Myc/His were inserted into pFastBac Dual (Invitrogen). Nct-V5/His and Pen-2 were inserted into pBlueBac4.5 as described (13, 14). Maintenance of embryonic fibroblast obtained from *PS1/PS2* double knock-out mice (DKO cells), viral packaging in Plat-E cells, retroviral infection, and generation of stable infectant pools were performed as described previously (12, 15). γ-Secretase complex was reconstituted in *Spodoptera frugiperda* Sf9 insect cells as described previously (13, 14). Briefly, P3 virus stock for each subunit was simultaneously added to adherent culture of Sf9 cells in a 75-cm^2 flask and collected 72 h later.

Antibodies and Immunochemical Analyses—Anti-G1L3 and PNT3 antibodies against GST-fused human PS1 loop or a synthetic peptide corresponding to the N-terminal 26 amino acids of human/mouse Pen-2, respectively, have been previously described (16, 17). Anti-$PS1_{NT}$ antibody was kindly provided by Dr. G. Thinakaran (The University of Chicago, Chicago, IL) (18). Other antibodies were purchased from Chemicon (anti-PS1 loop (MAB5232)), Covance (anti-Aph-1aL (O2C2)), or Sigma (anti-Nct (N1660)). Membrane fractionation, immunoblot analysis, and immunoprecipitation of CHAPSO-solubilized lysates were performed as described previously (7, 19, 20). 1% digitonin-solubilized cell lysates were analyzed by Blue Native-PAGE as per the manufacturer's instructions (10).

Photoaffinity Labeling—31C and 31C-Bpa were kindly provided by Drs. N. Umezawa and T. Higuchi (Nagoya City University, Nagoya, Japan) (21). pep.11 and pep.11-Bt (22) were purchased from Ito Life Sciences (Moriya, Japan) and BEX (Tokyo, Japan), respectively. Photoaffinity labeling was performed as described (12, 23, 24) with minor modifications. Briefly, membrane fractions were incubated with the indicated compounds and collected by centrifugation after UV irradiation. The pellets were solubilized by 1% SDS buffer, and streptavidin-Sepharose (GE Healthcare) was added to the supernatants to pull down the biotinylated proteins. Samples were then analyzed by immunoblotting.

SCAM—Membrane fractions with final protein concentration at 0.3 mg/ml (DKO cells) or 0.1 mg/ml (Sf9 cells) were incubated with *N*-biotinaminoethyl methanethiosulfonate (MTSEA-biotin) (Toronto Research Chemicals, Toronto, Canada) for 10 min at 37 °C. MTSEA-biotin was dissolved in dimethyl sulfoxide (DMSO) at 10 mM and stored at −80 °C until use. Concentration of MTSEA-biotin was shown in each figure. The reaction was terminated by centrifugation. The subsequent procedure was done as described (7–10). Briefly, biotinylated PS1 was captured by streptavidin-Sepharose (GE Healthcare) and eluted by boiling in Laemmli sample buffer containing 2-mercaptoethanol. Eluate was separated and subjected to immunoblot analysis using anti-PS1 antibodies. To estimate the SCAM ratio (see below) in a quantitative manner, we confirmed that each concentration of MTSEA-biotin did not reach saturation of the reaction.

Cysteine-based Cross-linking—Cross-linking experiment using 1,2-ethanediyl bismethanethiosulfonate (M2M) (Toronto Research Chemicals) was performed as described previously (7–9). In copper-phenanthroline (Cu-Phe) cross-linking experiments, membrane fractions were dissolved in 17 mM Tris-HCl (pH 8.0) buffer containing 1 mM $CaCl_2$, 100 mM NaCl, and Complete™ protease inhibitor mixture (Roche Applied Science). After the addition of $CuSO_4$ and 1,10-phenanthroline (final concentration at 3 and 15 mM, respectively), samples were incubated for 10 min at 4 °C. Reaction was terminated by the further addition of sample buffer containing 20 mM *N*-ethylmaleimide (NEM) and 10 mM EDTA and analyzed by immunoblot analysis.

RESULTS

Analysis of the Subunit Binding-defective PS1 Mutants—During the assembly of the γ-secretase, the subunits sequentially interact with PS to form an enzymatically active complex (5). Nct forms a subcomplex with Aph-1 and binds to the C terminus of PS1 (25, 26). Pen-2 directly associates at the WNF motif in TMD4 of PS to regulate the enzymatic activity (12, 27). We have previously found that PS1 mutant carrying alanine substitutions at the WNF motif (WNF mt) failed to interact with Pen-2. In this study, we also analyzed a PS1 mutant that lacks the C-terminal 12 amino acid residues (455st mt), the latter being the binding site for the Nct-Aph-1 subcomplex (26). We further designed a compound PS1 mutant in which both regions are mutated (WNF/455 mt) (Fig. 1*A*). Overexpression of wild-type (wt) PS1 in DKO cells resulted in the generation of PS fragments and recovered the levels of mature Nct and the accumulation of Pen-2, as described previously (Fig. 1*B*) (12). However, all PS1 mutants remained as a holoprotein and failed to restore the maturation of Nct. In addition, neither WNF nor WNF/455 mt rescued the expression of Pen-2. Immunoprecipitation analysis revealed that WNF and 455st mt failed to bind with Pen-2 and Nct-Aph-1aL, respectively, as described previously (Fig. 1*C*). Notably, WNF/455 mt was coprecipitated with neither of the subunits, indicating that the PS1 mutants lost the binding ability with specific subunits as designed. Formation of γ-secretase complex as a high molecular mass complex can be visualized by Blue Native-PAGE using 1% digitonin-solubilized cell lysates (Fig. 1*D*). In this analysis, γ-secretase complex was detected as an ~440-kDa band as described previously (12). WNF mt was also migrated at ~400–440 kDa as a doublet band, in which Nct and Aph-1aL were detected. However, consistent with the results of the immunoprecipitation experiment, no Pen-2 was detected, similarly to that in mock-transfected cells. The doublet band of this high molecular mass complex might represent a structural heterogeneity in conformation or binding mode to unidentified partner(s). In addition, an additional ~120-kDa-band that reacted only with anti-PS1 antibody appeared. In fact, this 120-kDa band was detected in all PS1-expressing cell lysates including WNF/445 mt-expressing cells. Thus, the 120-kDa band might represent the PS1 holoprotein without binding to known subunits. Further analysis would be needed to clarify whether the

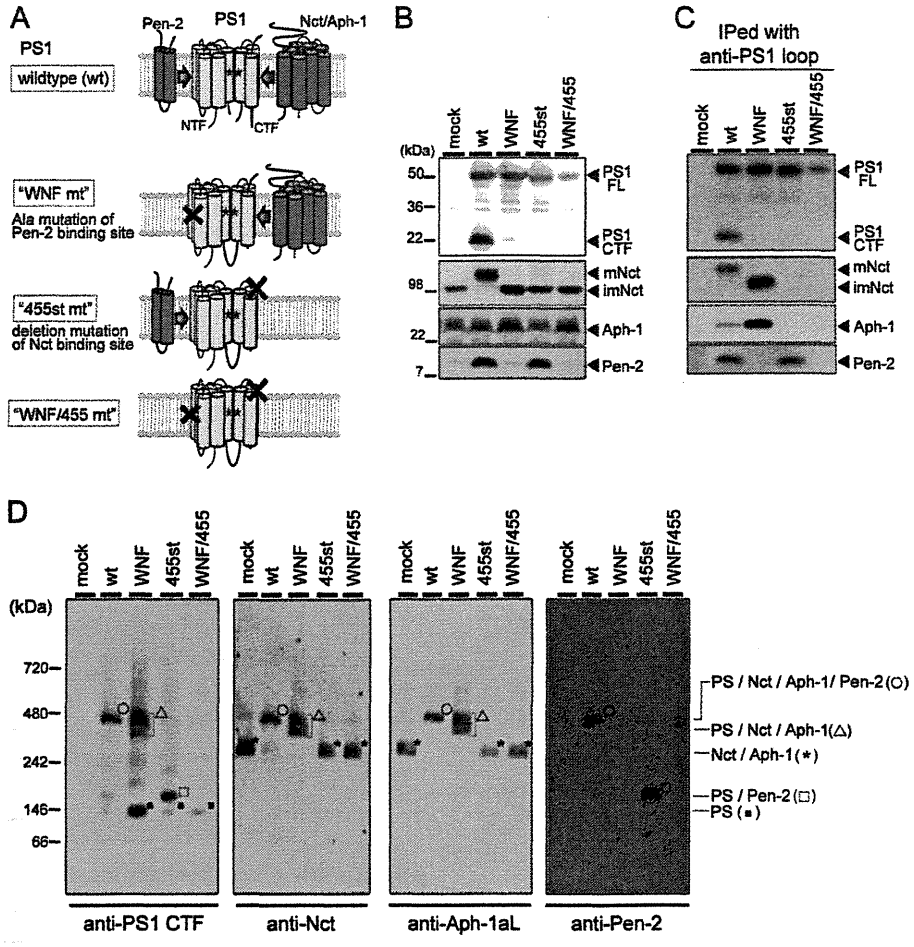

FIGURE 1. **Biochemical analysis of the subunit binding-defective PS1 mutants.** *A*, schematic representation of PS1 mutants used in this study. During the assembly of the γ-secretase, PS1 wild-type (*wt*) interacts with Nct-Aph-1 subcomplex and Pen-2 followed by endoproteolysis to generate PS1 NTF and CTF. *WNF mt* carries triple alanine substitutions at the Pen-2-binding WNF motif on TMD4 and interacts only with the Nct-Aph-1 subcomplex. *455st mt* lacks the 12 amino acids of the most C-terminal region, which is the binding site of the Nct-Aph-1 subcomplex, and interacts only with Pen-2. *WNF/455 mt* harbors a compound mutation of WNF mt and 455st mt. *B*, immunoblot analysis of DKO cells stably expressing wt PS1 or PS1 mt (as indicated above the panel). *FL*, full-length; *mNct*, mature Nct; *imNct*, immature Nct. *C*, complex formation of PS1 mutants. Immunoprecipitated samples (*IPed*) with Mab5232 antibody (anti-PS1 loop) were analyzed by immunoblotting. *D*, Blue Native-PAGE analysis of cell lysates solubilized with 1% digitonin. Molecular mass and content of the complex were indicated at the *left* and *right*, respectively, of the panel. Antibodies used for detection were G1L3 (anti-PS1 CTF), N1660 (anti-Nct), O2C2 (anti-Aph-1aL), and PNT3 (anti-Pen-2).

120-kDa PS1 holoprotein corresponds to the monomeric or dimeric forms of PS1 or PS1 complexed with unknown partner(s). In lysate of cells expressing 455st mt, PS1-Pen-2 complex was mainly detected as a 160-kDa band. However, the migration pattern of the 270-kDa band that reacted with anti-Nct as well as Aph-1aL antibodies was almost similar to that in mock-infected cells. This is consistent with the finding that C-terminal deletion mutation in PS1 diminished its binding with Nct-Aph-1 subcomplex.

To test whether the PS mutants formed an enzymatically active structure without the subunits, we took the photoaffinity labeling approach (10, 21). PS1 in an active γ-secretase complex harbors the catalytic and the initial substrate-binding sites, which are targeted by the transition state analog-type and the helical peptide-type γ-secretase inhibitors, respectively. 31C-Bpa, a transition state analog-type probe (28), was bound to wt PS1 NTF as well as CTF (Fig. 2), in agreement with previous studies (10, 21, 28). In contrast, neither wt PS1 holoprotein nor the subunit binding-incompetent PS1 mutants specifically bound to 31C-Bpa. A similar result was obtained using pep.11-Bt, which targeted exclusively PS1 NTF (10, 22). These results suggested that association of all subunits is required for the formation of both catalytic and initial substrate-binding sites in PS.

Effects of the Subunit Binding on the Water Accessibility to the Catalytic Pore of PS1—The results of the photoaffinity labeling experiments prompted us to examine the structural change of the catalytic pore in PS1 mutants. The catalytic pore structure within the membrane was assessed by thiol-based chemistry in SCAM (7, 8). Cys-less PS1 (PS1/Cys(−))-based subunit-binding mutants (WNF, 455st, WNF/455) also failed to form an enzymatically active high molecular mass complex (data not shown). We then constructed mutant PS1/Cys(−) having a single cysteine residue at the residues facing the catalytic pore in PS1 CTF (*i.e.* L383C, I387C, L435C, S438C, L443C, and Y446C) and examined the water accessibility of the substituted Cys residues by specific labeling using MTSEA-biotin (Fig. 3*D*). We also analyzed the residues located at the hydrophilic loop

(H351C, A398C) as controls. All cysteine mutants were specifically biotinylated. Intriguingly, in addition to PS1 CTF that represents the enzymatically active form, PS1 holoprotein was also labeled by MTSEA-biotin. This suggested that a pore-like structure has already been formed with the holoprotein form of PS1, consistent with the previous finding that PS holoprotein functions as a Ca^{2+} leak channel in endoplasmic reticulum (29). Moreover, the amount of biotinylated holoprotein was larger than that of CTF bound to MTSEA-biotin. Different biotinylation levels in holoprotein and fragment were also observed in L250C, which directly faces the pore on the NTF (Fig. 3*B*). We routinely detected some degradation bands just under the holoproteins (*i.e.* 40–45-kDa bands) in PS DKO cell lysates due to overexpression, as shown in Fig. 1*B*. These bands were also labeled by MTSEA-biotin. Furthermore, we tested the water accessibility of Cys-419, which is located in a hydrophobic environment and was never biotinylated in wt PS1 CTF. However, no labeling was observed in C419C holoprotein nor CTF (Fig. 3*C*). To compare the labeling efficiency in the holoprotein and the fragment forms of PS1, we defined the SCAM ratio as the biotinylated PS1 levels divided by the total PS1 levels in the input fraction (Fig. 4). The SCAM ratio of L383C holoprotein was 0.92 ± 0.43. In contrast, the SCAM ratio of L383C CTF was 0.13 ± 0.04 ($n = 3$, mean ± S.E., $p < 0.05$ by Student's t test), suggesting that the water accessibility of Leu-383 was significantly decreased in CTF. In addition, similar trends were detected in all mutants except for H351C, in which cysteine is located at the cytoplasmic hydrophilic loop 6. Notably, the SCAM ratio of A398C was also decreased in CTF, implicating the structural change of the loop region connected with TMD7 and TMD8. These results suggested that the microenvironment of the residues facing the catalytic pore as well as Ala-398 was altered in the fragment form of PS1.

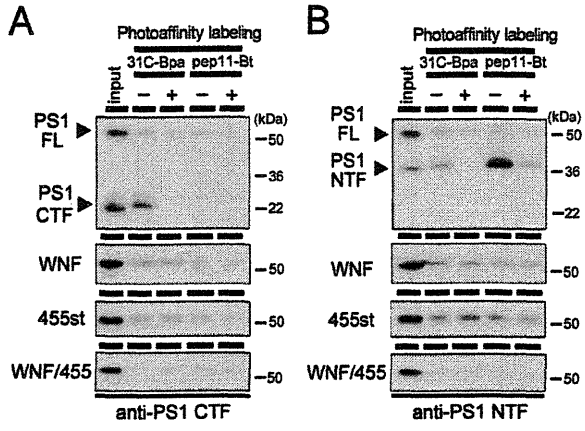

FIGURE 2. **Photoaffinity labeling experiment of PS1 mutants.** Microsome fractions of DKO cells stably expressing PS1 mutant were incubated with 31C-Bpa or pep.11-Bt in the presence (+) or absence (−) of parent compound 31C or pep.11, respectively. After 1 h of UV irradiation, samples were lysed with 1% SDS/PBS and incubated with streptavidin-Sepharose beads. Eluates were analyzed by immunoblotting using G1L3 (anti-PS1 CTF) (*A*) and $PS1_{NT}$ (anti-PS1 NTF) (*B*). The loaded amount of input was 6.5% relative to labeled fraction. Note that only PS1 fragments (NTF and CTF), but not PS1 holoprotein, were specifically labeled by both probes. *FL*, full-length.

Next we analyzed the effects of the subunit binding-incompetent mutations on the water accessibility of the residues facing the pore. The SCAM ratio of L383C in the subunit-binding mutants was almost comparable with that of wt PS1 holopro-

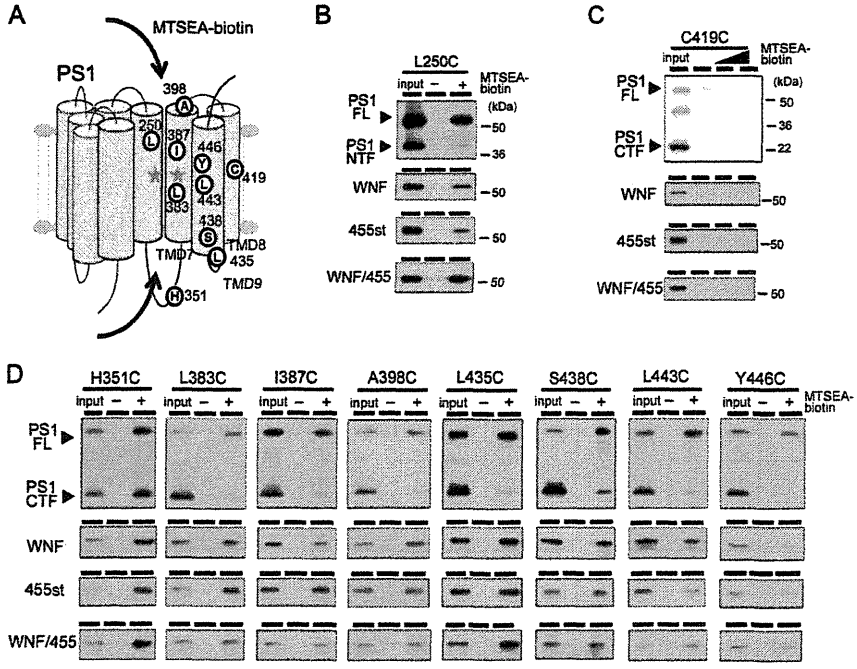

FIGURE 3. **SCAM analysis of PS1 mutants.** *A*, schematic representation of residues in PS1 analyzed in this study. The *letters* in *white circles* indicate the residues that are substituted to cysteine. *Gray stars* denote the catalytic center aspartates. In this preparation, MTSEA-biotin had access to Cys residues from both the extracellular and the intracellular sides (*arrows*). *B–D*, SCAM analysis of PS1 mts carrying Cys substitutions at NTF (*B*) or CTF (*C* and *D*). *Minus* and *Plus* denote samples incubated without or with MTSEA-biotin, respectively. Final concentration of MTSEA-biotin was 6.6 μM for L250C and S438C and 3.3 μM for other Cys mutants. Biotinylated proteins were precipitated by streptavidin beads, and the entire eluate was analyzed by immunoblotting. The loaded amount of input was 6.5% relative to labeled fraction. *C*, labeling to C419C mt by MTSEA-biotin at 0, 10, and 100 μM as denoted above the lanes. PS1 was detected by immunoblotting using $PS1_{NT}$ (anti-PS1 NTF) (*B*) and G1L3 (anti-PS1 CTF) (*C* and *D*). *FL*, full-length.

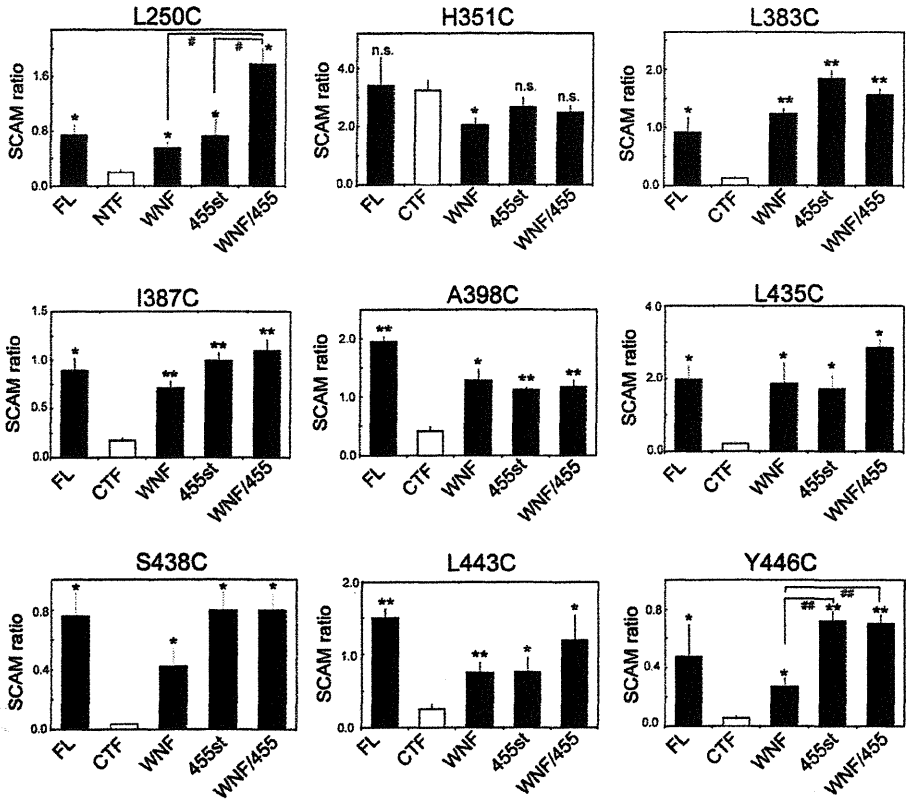

FIGURE 4. **Quantification of SCAM analysis on PS1 mutants.** Quantification of SCAM ratio by densitometric analysis of each band as shown in Fig. 3 was performed. SCAM ratio was calculated as the ratio of each PS1 polypeptide in MTSEA-biotin (+) to that in the input. *, $p < 0.05$; **, $p < 0.01$ (Student's *t* test, n = 3–8, mean ± S.E. when compared with that of NTF or CTF (*white bar*)); #, $p < 0.05$; ##, $p < 0.01$ (Student's *t* test, n = 3–8, mean ± S.E., sample pairs indicated by *lines*). *FL*, full-length; *n.s.*, not significant.

tein (*i.e.* WNF, 1.25 ± 0.15; 455st, 1.85 ± 0.33; WNF/455, 1.57 ± 0.25, n = 3–6) (Fig. 4), suggesting that the water accessibility of Leu-383 in holoprotein form was almost the same as that in the subunit-binding mutants. Similar results were obtained in all single cysteine PS1 mutants except for H351C. These results suggested that the complex assembly caused reduction in water accessibility around the residues facing the catalytic pore. Notably, the SCAM ratio of Y446C/WNF mt (0.27 ± 0.16) was lower than that of 455st mt (0.72 ± 0.11) or WNF/455 mt (0.71 ± 0.10). However, the SCAM ratio of Y446C CTF was much lower (0.06 ± 0.03), raising the possibility that the water accessibility in Tyr-446 was differently affected by binding of Nct-Aph-1 or Pen-2. In addition, the SCAM ratio of L250C/WNF mt (0.56 ± 0.09) as well as of L250C/455st mt (0.73 ± 0.23) was significantly lower than that of L250C/WNF/455 mt (1.78 ± 0.40), suggesting that binding of either of the subunits decreased the water accessibility of L250C. No subunit-binding mutant carrying C419C mutation was labeled by MTSEA-biotin, indicating that the subunit-binding mutations did not alter the general topology and conformation of PS1 (Fig. 3*C*). To examine whether increased water accessibility reflected the misfolded conformation of PS1 polypeptides, we conducted SCAM analysis after heating the cell lysates to induce misfolding. However, preincubation at 50 or 70 °C lowered the labeling efficiency of mutant PS1 holoproteins (*i.e.* I387C WNF/455 and L435C WNF/455) (Fig. 5*A*), indicating that increased water accessibility was not correlated with the misfolded conformation of PS1.

Finally, to test whether the changes in the SCAM ratio were caused by the allosteric effect of WNF or 455st mutation, we analyzed the recombinant PS1 proteins expressed in Sf9 cells (13, 14). We previously reported that Sf9 cells do not have detectable levels of endogenous γ-secretase (13). Co-expression of human PS1, Nct, Aph-1, and Pen-2 in Sf9 cells resulted in the reconstitution of functional γ-secretase complex, whereas single infection of PS1 did not show any γ-secretase activity (13). PS1 Cys(−) expressed with other subunits was endoproteolyzed, but neither PS1 holoprotein nor CTF was labeled by MTSEA-biotin (Fig. 5*B*). In contrast, both holoprotein and CTF of L383C expressed with other subunits were biotinylated (Fig. 5*B*). The SCAM ratio of PS1 CTF was lower (0.31 ± 0.05) than that of the holoprotein (1.34 ± 0.22) in a similar fashion to that observed in DKO cells (Fig. 5*C*). Notably, the SCAM ratio of L383C infected without other subunits was retained at a high level (1.52 ± 0.43) comparable with that of holoprotein in L383C with other subunits. This result supports our view that the change of the water accessibility was induced by the binding of other subunits, but not by the introduction of the subunit binding-defective mutations. Collectively, these data suggest that the hydrophilic pore structure in PS1 has already been formed without binding of the subunits and that the water accessibility of the pore is reduced by the complex assembly.

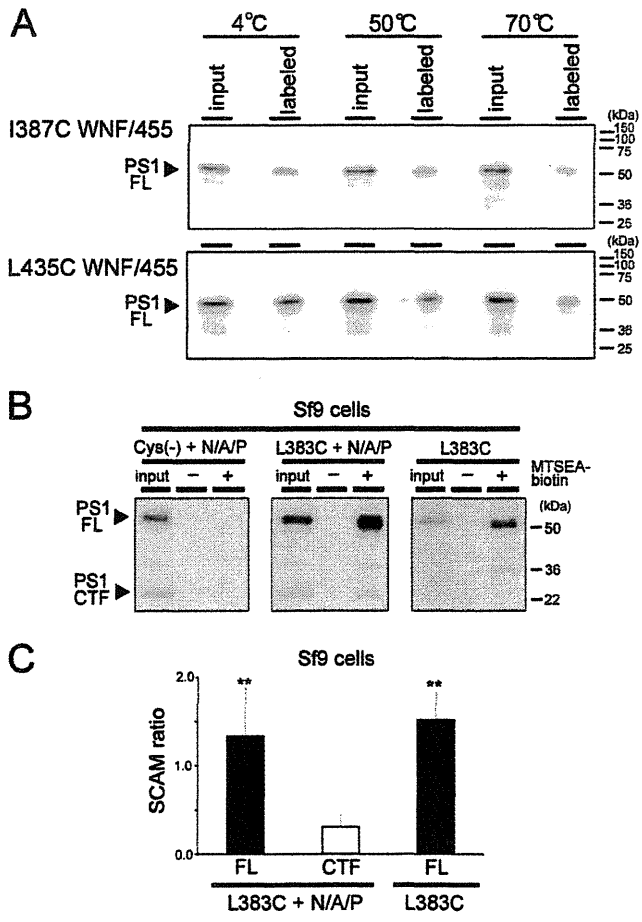

FIGURE 5. **SCAM analysis of misfolded PS1 and recombinant PS1.** *A*, temperature-dependent changes in labeling efficiency. Membrane fractions were incubated at the indicated temperatures for 10 min before SCAM analysis using MTSEA-biotin (3.3 μM, 10 min at 37 °C). G1L3 (anti-PS1 CTF) was used to immunodetection. *FL*, full-length. *B*, SCAM analysis of reconstituted γ-secretase in Sf9 cells. + *N/A/P* indicates co-infection of Nct-V5/His, Aph-1aL-Myc/His, and Pen-2. Final concentration of MTSEA-biotin was 3.3 μM. The loaded amount of input was 6.5% relative to the labeled fraction. *C*, quantification of the SCAM ratio in *B*. PS1 was detected by immunoblotting using G1L3 (anti-PS1 CTF) *, $p < 0.05$; **, $p < 0.01$ (Student's *t* test, $n = 3–8$, mean ± S.E. when compared with that of CTF (*white bar*)).

Effects of the Subunit Binding to the Proximity between Transmembrane Domains of PS1—Decreased water accessibility of the residues within the pore would be caused by the steric hindrance by the subunits or the conformational change of TMDs involved in the formation of the pore. To test the latter possibility, we conducted disulfide cross-linking experiments to detect the proximity between TMDs using two different reagents. M2M is a sulfhydryl-to-sulfhydryl MTS cross-linking reagent with spacer arms of 5.2 Å long (7, 30). Copper and 1,10-phenanthroline (Cu-Phe) acts as a redox catalyst to oxidize free sulfhydryls and form a disulfide bond in cysteines that can collide (31). We chose a cysteine pair at Leu-250 and Leu-435 located at the PS1 TMD6 and PALP motif, respectively, within the catalytic pore (Fig. 6*A*) (7, 8). Using M2M, the cross-linked NTF and CTF were observed in cell lysates expressing L250C/L435C, as described previously (Fig. 6*B*) (8). Moreover, Cu-Phe treatment resulted in an appearance of the NTF/CTF heterodimer, which was abolished by pretreatment with NEM. In fact, a small amount of NTF/CTF heterodimer, which was abolished by NEM pretreatment, was observed in the lysate without any cross-linking reagent. The mobilities of cross-linked products were slightly distinct, presumably due to difference in the structural flexibility of NTF/CTF heterodimer by M2M and Cu-Phe treatments. In contrast, no cross-linked product was observed in cell lysates expressing the single cysteine mutant (*i.e.* L250C and L435C) (Fig. 6*C*), indicating that Leu-250 and Leu-435 are located in a close proximity within the pore. Next we tested the effect of the subunit-binding mutations. Notably, no PS1 mutant was cross-linked by Cu-Phe treatment, whereas these mutants were cross-linked by M2M (Fig. 6*D*). Finally, to examine the effect of the endoproteolysis of PS1 on the proximity of these residues, we tested the M292D mutation, which is known to block endoproteolysis without affecting the complex formation and the enzymatic activity of the γ-secretase (32). Again, a cross-linked product of L250C/L435C with the M292D mutation was observed by both Cu-Phe and M2M treatment similarly to that in PS1/Cys(−) (Fig. 6*E*). This result suggested that the formation of an enzymatically active complex, but not the endoproteolysis, is the prerequisite to maintain the close proximity of Leu-250 and Leu-435 within the pore. These data suggest that the hydrophilic pore structure of PS1 has already been formed prior to binding of any subunits and that the subunit binding is correlated with the reduction of the water accessibility as well as the formation of the catalytic structure of the pore.

DISCUSSION

In this study, we analyzed the effects of the γ-secretase subunits on the structure of PS1 using chemical biology approaches. SCAM analysis revealed that water-accessible pore structure has already been formed by PS1 alone, the latter being an enzymatically inactive form (Fig. 3). Importantly, an increased SCAM ratio was observed in both the subunit binding-defective mutant PS1 as well as recombinant PS1 holoprotein singly expressed without other subunits. These results suggest that the binding of the subunits renders the pore structure narrower to form an enzymatically active catalytic site within the pore. Supporting this notion, Fluorescence-lifetime imaging microscopic analysis revealed that the interaction with different isoforms of Aph-1 or mutant Pen-2 affected the distance between PS1 NTF and CTF (33, 34). To date, several different functions of the γ-secretase subunits have been suggested: activity modulation, substrate recognition, trafficking, and stabilization of the enzyme (35). Here, our data suggest that in addition to these known functions, the subunits harbor a "chaperone"-like function acting on the arrangement of TMDs of PS during the assembly of the complex. Several ion or protein channels form a membrane protein complex containing auxiliary subunits. In SecYEG complex, a translocon in bacteria, SecY is a pore-forming subunit (36). SecE, which partly participates in the pore structure, is required for the stabilization of SecY. SecG is not essential for protein translocation, but stimulates preprotein translocation. X-ray crystallographic analysis revealed that the transmembrane segment of SecE embraces the SecY subunit as a clamp (37). Moreover, the function of voltage-dependent K^+ channels is regulated by voltage-gated

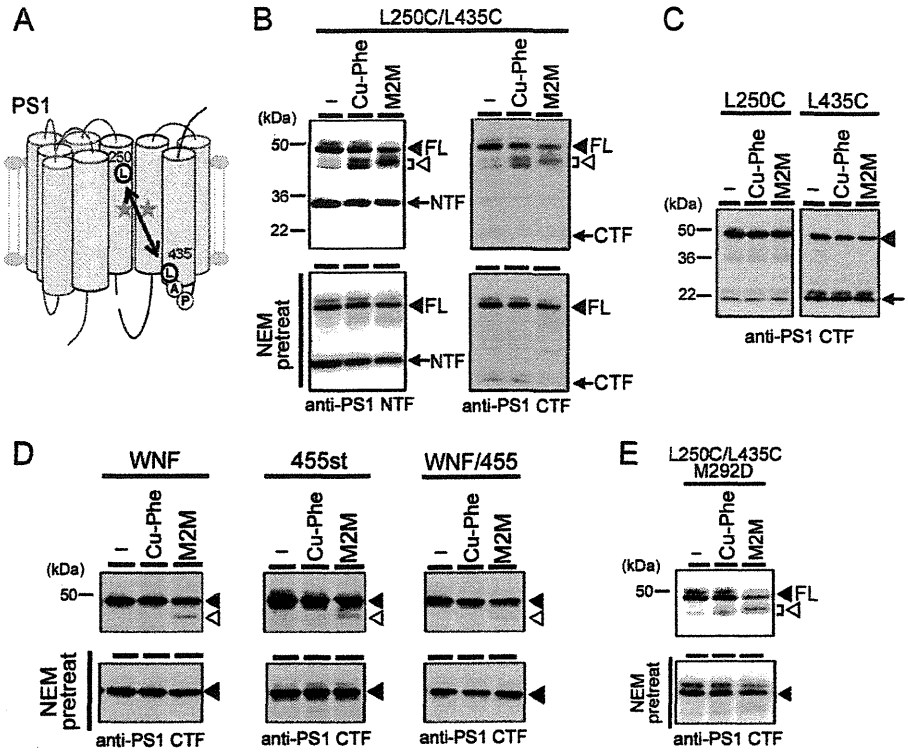

FIGURE 6. **Cross-linking analysis of PS1 mutants.** *A*, schematic representation of Leu-250 and Leu-435 in PS1. The *letters* in *white circles* with *thicker line* indicate the residues that are substituted to cysteine. *Gray stars* denote the catalytic center aspartates. In this preparation, MTSEA-biotin had access to Cys residues from both the extracellular and the intracellular sides. *B*, chemical cross-linking of PS1/Cys(−) mutant carrying L250C/L435C mutations. Microsome fractions of DKO cells stably expressing PS1 mt were treated with Cu-Phe or M2M at 4 °C and analyzed by immunoblotting. The *lower panel* shows the result using samples pretreated with NEM (*NEM pretreat*). *Black arrowheads* and *arrows* denote PS1 holoprotein and fragments, respectively. *White arrowheads* indicate cross-linked NTF/CTF heterodimer. NEM pretreatment significantly reduced the amount of cross-linked products. *FL*, full-length. *C*, cross-linking experiment using PS1/Cys(−) with single cysteine substitution. *D*, cross-linking experiment of WNF, 455st, and WNF/455 mt carrying L250C/L435C substitutions. The *lower panels* show the results using NEM-pretreated lysates. Note that cross-linked PS1 mutants were detected only in M2M-treated samples in these mutants. *E*, chemical cross-linking of M292D mutant carrying L250C/L435C. PS1 was detected by immunoblotting with $PS1_{NT}$ (anti-PS1 NTF) (*B*) and G1L3 (anti-PS1 CTF) (*B–E*).

potassium channel-interacting protein (KChIP) subunits (20, 38). Structural study indicated that the binding of voltage-gated potassium channel-interacting protein affected the gating kinetics as well as the stability of the pore-forming α-subunit of the channel (39). These data suggest that the auxiliary subunits harbor chaperone-like activity to affect the structure of the water-filled cavity within the membrane of the functional subunit in these channel structures. Importantly, we found that some residues in PS1 were differently affected by the binding of distinct subunits, whereas the hydrophilicity of residues around the pore was similarly affected in all mutants tested. The biotinylation of Y446C was significantly decreased only in the WNF mutant PS1, which can interact with Nct-Aph-1 (Fig. 4*E*). This result is consistent with the finding that Nct-Aph-1 interacts with PS1 CTF (25, 26, 40). Intriguingly, it has been shown that a point mutation at TMD9 rendered PS1 enzymatically active without binding to Nct (41). These results support our notion that the structure of TMD9 was affected by binding of the Nct-Aph-1 subcomplex. In addition, we found that the water accessibility of L250C was slightly decreased either in WNF or 455st mt when compared with that in the compound mt PS1. However, the SCAM ratios of these mutants were higher than that in L250C NTF. This suggests that the binding of Pen-2 directly to the TMD4 within PS1 NTF (12) affected the structure of TMD6

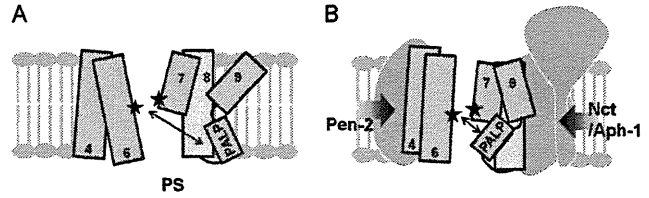

FIGURE 7. **Proposed model for the formation of the catalytic pore of PS1.** *A*, PS1 TMDs are shown as *columns* with *numbers*. Without any subunits, PS forms a relatively open pore structure within the membrane. *B*, upon the binding of subunits, the catalytic structure is activated by the structural changes in PS TMDs, and the PALP motif moves to the proximity to the catalytic center.

in NTF. In accordance with these results, it has been shown that recombinant Pen-2 activated the PS1 holoprotein in a proteoliposome preparation (42), suggesting that Pen-2 directly modulates the structure of the catalytic structure of PS1. In contrast, no direct interaction between NTF and Nct-Aph-1 has so far been reported. Thus, the reduction of the SCAM ratio of L250C NTF in the WNF mt background would reflect the steric hindrance induced by structural changes within CTF. Nevertheless, these data support the notion that the pore-like structure around the catalytic center formed by PS1 TMDs is closely regulated by the γ-secretase subunits (Fig. 7).

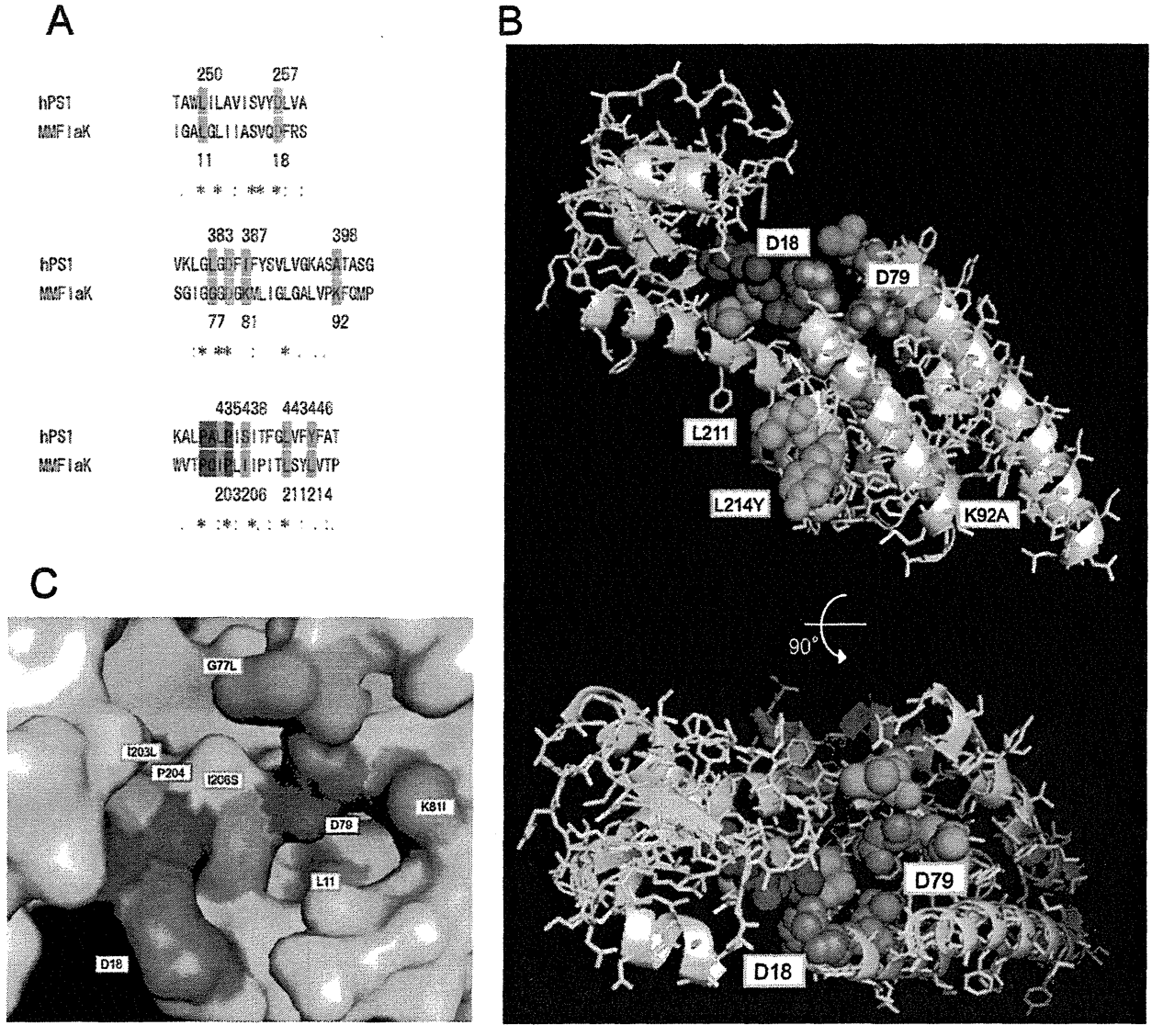

FIGURE 8. **Modified FlaK structural model replaced with the corresponding residues of PS1.** *A*, sequence alignment of *Homo sapiens* PS1 (*hPS1*) and *Methanococcus maripaludis* C6 FlaK around the catalytic and PALP motifs by ClustalW. The *numbers* of *colored residues* in PS1 and FlaK are shown above and below sequences, respectively. *Asterisks*, *colons*, and *periods* denote identical, conserved, and semiconserved residues in ClustalW. *B*, modified structural model of FlaK (Protein Data Bank (PDB) 3S0X) viewed from the cytosol (46). Colored residues were replaced with the corresponding amino acid residues in PS1 sequence (*A*) using PyMOL. The highlighted residues are shown as *spheres*, and other residues are shown as *gray ribbons* and *sticks*. *C*, closer view surface presentation around the catalytic site of the model.

Structural regulation of the disordered catalytic site in zymogen is an essential activation mechanism in several proteases such as trypsin, caspase, and calpain (43–45). Our cross-linking data suggest that the distance between Leu-250 and Leu-435 of PS1, which are located in proximity to the catalytic aspartates (7, 8), is altered by the assembly leading to the activation of the enzyme. Leu-250 on TMD6 is a highly conserved residue beyond species and functions as a subsite of the catalytic structure. Helical alignment of TMD6 suggests that Leu-250 locates on the same interface as Ala-246 and Asp-257 on the pore-facing α-helix. Leu-435 is a part of PALP motif in TMD9, which also participates in the formation of the catalytic site (46, 47). Intriguingly, NMR analysis revealed that TMD9 is a highly flexible domain in PS1 CTF (48). Thus, we propose a model in which PALP motif at the cytoplasmic side of TMD9 moves up to be located in proximity with the catalytic aspartates by the binding of PS1 to the subunits (Fig. 7). This structural arrangement of the catalytic site is highly reminiscent of the movement of the plug structure in SecY by SecE interaction (37). Intriguingly, classical proteases are activated by cleavage of their prodomain after acquiring the functionally active conformation. In this regard, it is tempting to speculate that the hydrophilic loop region of PS could represent an autoinhibitory domain of the γ-secretase (49, 50). However, endoproteolytic cleavage at the loop is dispensable for the activation of PS (32), supporting our notion that the allosteric changes of the structure of the catalytic pore by the subunit binding are critical for the acquisition of the proteolytic activity. Recently, crystallographic structural analysis of the first GxGD-type membrane protease FlaK has been reported (51). Notably, the catalytic

aspartates sit in distant locations within the open cavity. Considering the predicted catalytic mechanism of the aspartic protease, these aspartates should locate in proximity to each residue in an enzymatically active conformation. We compared the location of the residues in FlaK structure with that corresponding to the analyzed residues in our study (Fig. 8). Essentially, almost all tested residues seemed to face a single cavity where the catalytic aspartates reside. Thus, our results suggested that the conformation with the open cavity could be a common inactive structure of GxGD-type protease. Structural analysis of the active form of FlaK with transition state analog-type inhibitor would provide further structural information. In conclusion, we propose the first detailed structural rearrangement in TMDs of PS1 induced by binding of the γ-secretase subunits during the assembly of the γ-secretase complex. This result also raised the possible chaperone-like function of the subunits during the assembly as well as the activation of γ-secretase complex. Further structural analyses (*i.e.* x-ray crystallography, NMR, molecular dynamics simulation) would pave the way to deeper understanding of the functions of the subunits as well as the structural changes in PS1 in the activation process of the γ-secretase complex.

Acknowledgments—We are grateful to Drs. N. Umezawa and T. Higuchi (Nagoya City University) and Dr. G. Thinakaran (The University of Chicago) for valuable reagents and to our current and previous laboratory members for helpful discussions and technical assistance.

REFERENCES

1. Holtzman, D. M., Morris, J. C., and Goate, A. M. (2011) Alzheimer disease: the challenge of the second century. *Sci. Transl. Med.* **3,** 77sr1
2. Tomita, T. (2009) Secretase inhibitors and modulators for Alzheimer disease treatment. *Expert Rev. Neurother* **9,** 661–679
3. Iwatsubo, T., Odaka, A., Suzuki, N., Mizusawa, H., Nukina, N., and Ihara, Y. (1994) Visualization of Aβ42(43) and Aβ40 in senile plaques with end-specific Aβ monoclonals: evidence that an initially deposited species is Aβ42(43). *Neuron* **13,** 45–53
4. Erez, E., Fass, D., and Bibi, E. (2009) How intramembrane proteases bury hydrolytic reactions in the membrane. *Nature* **459,** 371–378
5. Takasugi, N., Tomita, T., Hayashi, I., Tsuruoka, M., Niimura, M., Takahashi, Y., Thinakaran, G., and Iwatsubo, T. (2003) The role of presenilin cofactors in the γ-secretase complex. *Nature* **422,** 438–441
6. Edbauer, D., Winkler, E., Regula, J. T., Pesold, B., Steiner, H., and Haass, C. (2003) Reconstitution of γ-secretase activity. *Nat. Cell Biol.* **5,** 486–488
7. Sato, C., Morohashi, Y., Tomita, T., and Iwatsubo, T. (2006) Structure of the catalytic pore of γ-secretase probed by the accessibility of substituted cysteines. *J. Neurosci.* **26,** 12081–12088
8. Sato, C., Takagi, S., Tomita, T., and Iwatsubo, T. (2008) The C-terminal PAL motif and transmembrane domain 9 of presenilin 1 are involved in the formation of the catalytic pore of the γ-secretase. *J. Neurosci.* **28,** 6264–6271
9. Takagi, S., Tominaga, A., Sato, C., Tomita, T., and Iwatsubo, T. (2010) Participation of transmembrane domain 1 of presenilin 1 in the catalytic pore structure of the γ-secretase. *J. Neurosci.* **30,** 15943–15950
10. Watanabe, N., Takagi, S., Tominaga, A., Tomita, T., and Iwatsubo, T. (2010) Functional analysis of the transmembrane domains of presenilin 1: participation of transmembrane domains 2 and 6 in the formation of initial substrate-binding site of γ-secretase. *J. Biol. Chem.* **285,** 19738–19746
11. Tolia, A., Chávez-Gutiérrez, L., and De Strooper, B. (2006) Contribution of presenilin transmembrane domains 6 and 7 to a water-containing cavity in the γ-secretase complex. *J. Biol. Chem.* **281,** 27633–27642
12. Watanabe, N., Tomita, T., Sato, C., Kitamura, T., Morohashi, Y., and Iwatsubo, T. (2005) Pen-2 is incorporated into the γ-secretase complex through binding to transmembrane domain 4 of presenilin 1. *J. Biol. Chem.* **280,** 41967–41975
13. Hayashi, I., Urano, Y., Fukuda, R., Isoo, N., Kodama, T., Hamakubo, T., Tomita, T., and Iwatsubo, T. (2004) Selective reconstitution and recovery of functional γ-secretase complex on budded baculovirus particles. *J Biol Chem* **279,** 38040–38046
14. Ogura, T., Mio, K., Hayashi, I., Miyashita, H., Fukuda, R., Kopan, R., Kodama, T., Hamakubo, T., Iwatsubo, T., Iwastubo, T., Tomita, T., and Sato, C. (2006) Three-dimensional structure of the γ-secretase complex. *Biochem. Biophys. Res. Commun.* **343,** 525–534
15. Kitamura, T., Koshino, Y., Shibata, F., Oki, T., Nakajima, H., Nosaka, T., and Kumagai, H. (2003) Retrovirus-mediated gene transfer and expression cloning: powerful tools in functional genomics. *Exp. Hematol.* **31,** 1007–1014
16. Tomita, T., Takikawa, R., Koyama, A., Morohashi, Y., Takasugi, N., Saido, T. C., Maruyama, K., and Iwatsubo, T. (1999) C terminus of presenilin is required for overproduction of amyloidogenic Aβ42 through stabilization and endoproteolysis of presenilin. *J. Neurosci.* **19,** 10627–10634
17. Isoo, N., Sato, C., Miyashita, H., Shinohara, M., Takasugi, N., Morohashi, Y., Tsuji, S., Tomita, T., and Iwatsubo, T. (2007) Aβ42 overproduction associated with structural changes in the catalytic pore of γ-secretase: common effects of Pen-2 N-terminal elongation and fenofibrate. *J. Biol. Chem.* **282,** 12388–12396
18. Leem, J. Y., Vijayan, S., Han, P., Cai, D., Machura, M., Lopes, K. O., Veselits, M. L., Xu, H., and Thinakaran, G. (2002) Presenilin 1 is required for maturation and cell surface accumulation of nicastrin. *J. Biol. Chem.* **277,** 19236–19240
19. Tomita, T., Maruyama, K., Saido, T. C., Kume, H., Shinozaki, K., Tokuhiro, S., Capell, A., Walter, J., Grünberg, J., Haass, C., Iwatsubo, T., and Obata, K. (1997) The presenilin 2 mutation (N141I) linked to familial Alzheimer disease (Volga German families) increases the secretion of amyloid-β protein ending at the 42nd (or 43rd) residue. *Proc. Natl. Acad. Sci. U.S.A.* **94,** 2025–2030
20. Morohashi, Y., Hatano, N., Ohya, S., Takikawa, R., Watabiki, T., Takasugi, N., Imaizumi, Y., Tomita, T., and Iwatsubo, T. (2002) Molecular cloning and characterization of CALP/KChIP4, a novel EF-hand protein interacting with presenilin 2 and voltage-gated potassium channel subunit Kv4. *J. Biol. Chem.* **277,** 14965–14975
21. Imamura, Y., Watanabe, N., Umezawa, N., Iwatsubo, T., Kato, N., Tomita, T., and Higuchi, T. (2009) Inhibition of γ-secretase activity by helical β-peptide foldamers. *J. Am. Chem. Soc.* **131,** 7353–7359
22. Das, C., Berezovska, O., Diehl, T. S., Genet, C., Buldyrev, I., Tsai, J. Y., Hyman, B. T., and Wolfe, M. S. (2003) Designed helical peptides inhibit an intramembrane protease. *J. Am. Chem. Soc.* **125,** 11794–11795
23. Morohashi, Y., Kan, T., Tominari, Y., Fuwa, H., Okamura, Y., Watanabe, N., Sato, C., Natsugari, H., Fukuyama, T., Iwatsubo, T., and Tomita, T. (2006) C-terminal fragment of presenilin is the molecular target of a dipeptidic γ-secretase-specific inhibitor DAPT (*N*-[*N*-(3,5-difluorophenacetyl)-L-alanyl]-*S*-phenylglycine *t*-butyl ester). *J. Biol. Chem.* **281,** 14670–14676
24. Ohki, Y., Higo, T., Uemura, K., Shimada, N., Osawa, S., Berezovska, O., Yokoshima, S., Fukuyama, T., Tomita, T., and Iwatsubo, T. (2011) Phenylpiperidine-type γ-secretase modulators target the transmembrane domain 1 of presenilin 1. *EMBO J.* **30,** 4815–4824
25. Kaether, C., Capell, A., Edbauer, D., Winkler, E., Novak, B., Steiner, H., and Haass, C. (2004) The presenilin C terminus is required for ER retention, nicastrin binding, and γ-secretase activity. *EMBO J.* **23,** 4738–4748
26. Bergman, A., Laudon, H., Winblad, B., Lundkvist, J., and Näslund, J. (2004) The extreme C terminus of presenilin 1 is essential for γ-secretase complex assembly and activity. *J. Biol. Chem.* **279,** 45564–45572
27. Kim, S. H., and Sisodia, S. S. (2005) Evidence that the "NF" motif in transmembrane domain 4 of presenilin 1 is critical for binding with PEN-2. *J. Biol. Chem.* **280,** 41953–41966
28. Micchelli, C. A., Esler, W. P., Kimberly, W. T., Jack, C., Berezovska, O., Kornilova, A., Hyman, B. T., Perrimon, N., and Wolfe, M. S. (2003) γ-Secretase/presenilin inhibitors for Alzheimer disease phenocopy *Notch* mutations in *Drosophila*. *FASEB J.* **17,** 79–81

29. Tu, H., Nelson, O., Bezprozvanny, A., Wang, Z., Lee, S. F., Hao, Y. H., Serneels, L., De Strooper, B., Yu, G., and Bezprozvanny, I. (2006) Presenilins form ER Ca^{2+} leak channels, a function disrupted by familial Alzheimer disease-linked mutations. *Cell* **126,** 981–993
30. Loo, T. W., and Clarke, D. M. (2001) Determining the dimensions of the drug-binding domain of human P-glycoprotein using thiol cross-linking compounds as molecular rulers. *J. Biol. Chem.* **276,** 36877–36880
31. Klco, J. M., Lassere, T. B., and Baranski, T. J. (2003) C5a receptor oligomerization. I. Disulfide trapping reveals oligomers and potential contact surfaces in a G protein-coupled receptor. *J. Biol. Chem.* **278,** 35345–35353
32. Steiner, H., Romig, H., Pesold, B., Philipp, U., Baader, M., Citron, M., Loetscher, H., Jacobsen, H., and Haass, C. (1999) Amyloidogenic function of the Alzheimer disease-associated presenilin 1 in the absence of endoproteolysis. *Biochemistry* **38,** 14600–14605
33. Serneels, L., Van Biervliet, J., Craessaerts, K., Dejaegere, T., Horré, K., Van Houtvin, T., Esselmann, H., Paul, S., Schäfer, M. K., Berezovska, O., Hyman, B. T., Sprangers, B., Sciot, R., Moons, L., Jucker, M., Yang, Z., May, P. C., Karran, E., Wiltfang, J., D'Hooge, R., and De Strooper, B. (2009) γ-Secretase heterogeneity in the Aph1 subunit: relevance for Alzheimer disease. *Science* **324,** 639–642
34. Uemura, K., Lill, C. M., Li, X., Peters, J. A., Ivanov, A., Fan, Z., DeStrooper, B., Bacskai, B. J., Hyman, B. T., and Berezovska, O. (2009) Allosteric modulation of PS1/γ-secretase conformation correlates with amyloid-β(42/40) ratio. *PLoS One* **4,** e7893
35. De Strooper, B., and Annaert, W. (2010) Novel research horizons for presenilins and γ-secretases in cell biology and disease. *Annu. Rev. Cell Dev. Biol.* **26,** 235–260
36. du Plessis, D. J., Nouwen, N., and Driessen, A. J. (2011) The Sec translocase. *Biochim. Biophys. Acta* **1808,** 851–865
37. Van den Berg, B., Clemons, W. M., Jr., Collinson, I., Modis, Y., Hartmann, E., Harrison, S. C., and Rapoport, T. A. (2004) X-ray structure of a protein-conducting channel. *Nature* **427,** 36–44
38. Wang, K. (2008) Modulation by clamping: Kv4 and KChIP interactions. *Neurochem. Res.* **33,** 1964–1969
39. Wang, H., Yan, Y., Liu, Q., Huang, Y., Shen, Y., Chen, L., Chen, Y., Yang, Q., Hao, Q., Wang, K., and Chai, J. (2007) Structural basis for modulation of Kv4 K^+ channels by auxiliary KChIP subunits. *Nat. Neurosci.* **10,** 32–39
40. Steiner, H., Winkler, E., and Haass, C. (2008) Chemical cross-linking provides a model of the γ-secretase complex subunit architecture and evidence for close proximity of the C-terminal fragment of presenilin with APH-1. *J. Biol. Chem.* **283,** 34677–34686
41. Futai, E., Yagishita, S., and Ishiura, S. (2009) Nicastrin is dispensable for γ-secretase protease activity in the presence of specific presenilin mutations. *J. Biol. Chem.* **284,** 13013–13022
42. Ahn, K., Shelton, C. C., Tian, Y., Zhang, X., Gilchrist, M. L., Sisodia, S. S., and Li, Y. M. (2010) Activation and intrinsic γ-secretase activity of presenilin 1. *Proc. Natl. Acad. Sci. U.S.A.* **107,** 21435–21440
43. Fehlhammer, H., Bode, W., and Huber, R. (1977) Crystal structure of bovine trypsinogen at 1–8 Å resolution. II. Crystallographic refinement, refined crystal structure, and comparison with bovine trypsin. *J. Mol. Biol.* **111,** 415–438
44. Riedl, S. J., Fuentes-Prior, P., Renatus, M., Kairies, N., Krapp, S., Huber, R., Salvesen, G. S., and Bode, W. (2001) Structural basis for the activation of human procaspase-7. *Proc. Natl. Acad. Sci. U.S.A.* **98,** 14790–14795
45. Hosfield, C. M., Elce, J. S., Davies, P. L., and Jia, Z. (1999) Crystal structure of calpain reveals the structural basis for Ca^{2+}-dependent protease activity and a novel mode of enzyme activation. *EMBO J.* **18,** 6880–6889
46. Tomita, T., Watabiki, T., Takikawa, R., Morohashi, Y., Takasugi, N., Kopan, R., De Strooper, B., and Iwatsubo, T. (2001) The first proline of PALP motif at the C terminus of presenilins is obligatory for stabilization, complex formation, and γ-secretase activities of presenilins. *J. Biol. Chem.* **276,** 33273–33281
47. Wang, J., Beher, D., Nyborg, A. C., Shearman, M. S., Golde, T. E., and Goate, A. (2006) C-terminal PAL motif of presenilin and presenilin homologues required for normal active site conformation. *J. Neurochem.* **96,** 218–227
48. Sobhanifar, S., Schneider, B., Löhr, F., Gottstein, D., Ikeya, T., Mlynarczyk, K., Pulawski, W., Ghoshdastider, U., Kolinski, M., Filipek, S., Güntert, P., Bernhard, F., and Dötsch, V. (2010) Structural investigation of the C-terminal catalytic fragment of presenilin 1. *Proc. Natl. Acad. Sci. U.S.A.* **107,** 9644–9649
49. Knappenberger, K. S., Tian, G., Ye, X., Sobotka-Briner, C., Ghanekar, S. V., Greenberg, B. D., and Scott, C. W. (2004) Mechanism of γ-secretase cleavage activation: is γ-secretase regulated through autoinhibition involving the presenilin-1 exon 9 loop? *Biochemistry* **43,** 6208–6218
50. Fukumori, A., Fluhrer, R., Steiner, H., and Haass, C. (2010) Three-amino acid spacing of presenilin endoproteolysis suggests a general stepwise cleavage of γ-secretase-mediated intramembrane proteolysis. *J. Neurosci.* **30,** 7853–7862
51. Hu, J., Xue, Y., Lee, S., and Ha, Y. (2011) The crystal structure of GXGD membrane protease FlaK. *Nature* **475,** 528–531

Neuron
Article

Activity-Dependent Proteolytic Cleavage of Neuroligin-1

Kunimichi Suzuki,[1] Yukari Hayashi,[1] Soichiro Nakahara,[2] Hiroshi Kumazaki,[3] Johannes Prox,[5] Keisuke Horiuchi,[6] Mingshuo Zeng,[3] Shun Tanimura,[3] Yoshitake Nishiyama,[3] Satoko Osawa,[1] Atsuko Sehara-Fujisawa,[7] Paul Saftig,[5] Satoshi Yokoshima,[3] Tohru Fukuyama,[3] Norio Matsuki,[2] Ryuta Koyama,[2] Taisuke Tomita,[1,8,*] and Takeshi Iwatsubo[1,4,8]
[1]Department of Neuropathology and Neuroscience
[2]Laboratory of Chemical Pharmacology
[3]Laboratory of Synthetic Natural Products Chemistry, Graduate School of Pharmaceutical Sciences
[4]Department of Neuropathology, Graduate School of Medicine
The University of Tokyo, Hongo 7-3-1, Bunkyo, Tokyo 113-0033, Japan
[5]Institut für Biochemie, Christian-Albrechts-Universität zu Kiel, D-24098 Kiel, Germany
[6]Department of Orthopedic Surgery, School of Medicine, Keio University, Shinjuku, Tokyo 160-8582, Japan
[7]Department of Growth Regulation, Institute for Frontier Medical Sciences, Kyoto University, Sakyo-ku, Kyoto 606-8507, Japan
[8]Core Research for Evolutional Science and Technology, Japan Science and Technology Agency
*Correspondence: taisuke@mol.f.u-tokyo.ac.jp
http://dx.doi.org/10.1016/j.neuron.2012.10.003

SUMMARY

Neuroligin (NLG), a postsynaptic adhesion molecule, is involved in the formation of synapses by binding to a cognate presynaptic ligand, neurexin. Here we report that neuroligin-1 (NLG1) undergoes ectodomain shedding at the juxtamembrane stalk region to generate a secreted form of NLG1 and a membrane-tethered C-terminal fragment (CTF) in adult rat brains in vivo as well as in neuronal cultures. Pharmacological and genetic studies identified ADAM10 as the major protease responsible for NLG1 shedding, the latter being augmented by synaptic NMDA receptor activation or interaction with soluble neurexin ligands. NLG1-CTF was subsequently cleaved by presenilin/γ-secretase. Secretion of soluble NLG1 was significantly upregulated under a prolonged epileptic seizure condition, and inhibition of NLG1 shedding led to an increase in numbers of dendritic spines in neuronal cultures. Collectively, neuronal activity-dependent proteolytic processing of NLG1 may negatively regulate the remodeling of spines at excitatory synapses.

INTRODUCTION

Formation and maintenance of the synaptic structure is a dynamic process that requires bidirectional interactions between pre- and postsynaptic components. A diverse assortment of cell adhesion molecules is present at the synapse and organizes the synaptic specializations of both excitatory and inhibitory central synapses (Dalva et al., 2007; Siddiqui and Craig, 2011). Neuroligin (NLG) is one of the potent synaptogenic adhesion proteins located at the postsynapse, which transsynaptically binds to a presynaptic ligand, neurexin (NRX) (Ichtchenko et al., 1995; Irie et al., 1997; Scheiffele et al., 2000; Südhof, 2008; Bottos et al., 2011). Mammals express four NLG genes (i.e., NLG1 to NLG4). NLG polypeptides are type 1 transmembrane proteins with a large extracellular domain with homology to acetylcholinesterases but lack critical residues in the active site and interact with NRXs at the synaptic membrane surface (Südhof, 2008). Notably, NLG1 is localized at glutamatergic postsynapse, and overexpression of NLG1 induces the accumulation of glutamatergic presynapse and postsynapse molecules in vitro (Song et al., 1999; Scheiffele et al., 2000; Budreck and Scheiffele, 2007). In contrast, NLG2 triggers the maturation of GABAergic synapses, implicating specific functions of different NLGs in the formation and maturation of different chemical types of synapses in vitro and in vivo (Graf et al., 2004; Varoqueaux et al., 2004, 2006).

Recent studies revealed that copy number variation or point mutation in NLG genes are linked to autism spectrum disorder (ASD), schizophrenia, or mental retardation (reviewed in Südhof, 2008). Notably, ASD-linked mutations in NLG genes have been shown to affect the expression, folding, or dimerization of NLG proteins to compromise their surface expression and binding to NRXs (Comoletti et al., 2004; Levinson and El-Husseini, 2007; Zhang et al., 2009). Moreover, copy number variations that are associated with an increased risk of ASD were identified in NLG1 locus (Glessner et al., 2009). NLG1 knockout (KO) or transgenic mice showed synaptic dysfunctions and ASD-like behaviors (Varoqueaux et al., 2006; Chubykin et al., 2007; Blundell et al., 2010; Dahlhaus et al., 2010). Thus, the levels of NLGs within the synaptic membranes are presumed to directly modulate the synaptic functions in vivo. Although several reports indicated that the surface levels of NLG1 are regulated by synaptic activities through membrane trafficking (Schapitz et al., 2010; Thyagarajan and Ting, 2010), the regulatory mechanisms to control protein levels of NLG remains unclear. Here, we show that NLG1 is sequentially cleaved by ADAM10 and γ-secretase to release its extra- and intracellular domain fragments, respectively. Proteolytic processing of NLG1 resulted in the elimination of NLG1 on the cell surface, thereby causing a decrease in the

synaptogenic activity of NLG1. We further show that ADAM10-mediated shedding is regulated in an activity-dependent manner through NMDA receptor (NMDAR) activation or by binding to secreted forms of NRXs. Our present results suggest that neuronal activity and interaction with NRXs regulate the levels of NLG1 via proteolytic processing to modulate the adhesion system as well as the functions of synapses.

RESULTS

Proteolytic Processing of NLGs in Brains and Neuronal Cultures

NLGs are synaptogenic type 1 transmembrane proteins that harbor large extracellular domains (Ichtchenko et al., 1995). While the levels of NLGs are presumed to be correlated with their physiological and pathological functions (Varoqueaux et al., 2006; Chubykin et al., 2007; Glessner et al., 2009; Blundell et al., 2010; Dahlhaus et al., 2010), little information is available on the proteolytic mechanism of NLGs. Several lines of evidence have indicated that a subset of type 1 transmembrane proteins are processed by sequential cleavages by ectodomain shedding and intramembrane cleavage, the latter being executed by γ-secretase (Beel and Sanders, 2008; Bai and Pfaff, 2011). To test whether the levels of NLGs are regulated by proteolytic processing, we analyzed endogenous NLG polypeptides in adult rat brains (Figure 1A). Immunoblot analysis using antibodies that specifically recognize the cytoplasmic region of NLG1 and NLG2 (see Figure S1 available online) revealed immunopositive bands at ~20–25 kDa, in addition to full-length (FL) protein that migrated at ~120 kDa. Because the predicted sizes of the cytoplasmic domain of NLGs were within the range of 120–165 amino acid (aa) lengths (NLG1, 125 aa; NLG2, 137 aa), we reasoned that the ~20–25 kDa polypeptides represent the membrane-tethered C-terminal fragment (CTF) of endogenous NLGs. Multiple bands corresponding to CTFs may represent different posttranslational modifications (e.g., glycosylation, see below). To examine whether these CTFs are processed by the γ-secretase activity, we incubated the membrane fractions of rat brains at 37°C and detected the appearance of additional bands that migrate faster than the CTFs with each NLG. Moreover, addition of DAPT, a specific γ-secretase inhibitor, abolished the generation of the smaller CTFs, in a similar manner to that observed with a well-known γ-secretase substrate, amyloid precursor protein (APP). These data suggested that NLG-CTFs are cleaved by the γ-secretase activity to release the intracellular domain (ICD) (Figure 1B). In parallel with the generation of ICDs, we observed a significant reduction in NLG1-FL upon incubation, concomitant with the generation of a smaller NLG1 fragment, which was detected by an antibody against the extracellular region of NLG1 (Figure 1C). Generation of this extracellular fragment of NLG1 was decreased by treatment with metalloprotease inhibitors (i.e., EDTA, TAPI2), supporting the notion that the extracellular domain of NLG1 is processed by ectodomain shedding. To test whether this processing occurs at synapses under a physiological condition, we incubated synaptoneurosome preparation from adult mouse brain, which contains a population of purified presynaptic boutons attached to postsynaptic processes (Villasana et al., 2006; Kim et al., 2010) (Figures 1D and 1E). After ultracentrifugation after incubation, soluble NLG1 (sNLG1) as well as NLG1-ICD was detected in the soluble fraction, which was abolished by coincubation with TAPI2 and DAPT, respectively. To ascertain that these cleavages occur in situ in neuronal cultures, we analyzed cell lysates and conditioned media (CM) from mouse cortical primary neuronal cultures obtained from embryonic day (E) 18 pups by immunoblotting and detected the secretion of an ~98 kDa single polypeptide in the conditioned media, which migrated at an identical position to that generated upon incubation of the membrane fractions, by an antibody against the extracellular domain of NLG1 (Figures 1F and 1G). This band disappeared by treatment with metalloprotease inhibitors (i.e., GM6001, TAPI2). These data suggest that the extracellular domain of NLG1 is shed by the metalloprotease activity to release sNLG1 into the conditioned media. Furthermore, DAPT treatment caused the accumulation of CTFs of NLG1 as well as of NLG2. Notably, simultaneous administration of DAPT and metalloprotease inhibitors decreased the accumulation of the CTFs. However, endogenous NLG-ICD, which was observed upon incubation of microsomes from brain lysates, was hardly detectable in cell lysates from cultured primary neurons. This suggests that NLG-ICD is a highly labile endoproteolytic product. These findings led us to speculate that NLGs are initially processed by metalloprotease at the extracellular region to generate sNLG and membrane-tethered NLG-CTF, the latter being further cleaved by the γ-secretase activity (Figure 1H).

ADAM10 and γ-Secretase Are Responsible for the Proteolytic Processing of NLG1

Next we analyzed the metabolism of NLGs in mouse embryonic fibroblasts from *Psen1*$^{-/-}$/*Psen2*$^{-/-}$ double knockout mice (DKO cells), which completely lacks the γ-secretase activity (Herreman et al., 2000). Accumulation of NLG-CTFs was observed upon the overexpression of hemagglutinin (HA)-tagged NLGs in DKO cells (Figure 2A). However, the levels of the accumulated NLG-CTFs were significantly reduced by the coexpression of human PS1, indicating that γ-secretase activity is responsible for the processing of NLG-CTFs. ADAM10 is known as a responsible enzyme for ectodomain shedding of a subset of γ-secretase substrates (e.g., Notch, APP, cadherin, and CD44) at the membrane-proximal region of ectodomain (Saftig and Reiss, 2011). To test whether ADAM10 is involved in the processing of NLGs, we overexpressed HA-tagged NLG1 or NLG2 in murine embryonic fibroblasts (MEFs) obtained from ADAM10 knockout (*Adam10*$^{-/-}$) or heterozygous (*Adam10*$^{+/-}$) mice (Figure 2B) (Hartmann et al., 2002). In *Adam10*$^{-/-}$ MEF, the generation of sNLG1 was significantly reduced. In contrast, no change in NLG1 processing was observed in MEFs obtained from knockout mice of other ADAMs (i.e., *Adam8*$^{-/-}$, *Adam17*$^{-/-}$, *Adam19*$^{-/-}$, *Adam9*$^{-/-}$; *Adam12*$^{-/-}$;*Adam15*$^{-/-}$ [TKO]) (Zhou et al., 2004; Weskamp et al., 2006; Kawaguchi et al., 2007; Horiuchi et al., 2007). These data strongly suggest that ADAM10 is a responsible enzyme for the shedding of NLG1. Intriguingly, the level of soluble NLG2 secreted from *Adam10*$^{-/-}$ MEF was almost comparable to those from other ADAM knockout MEFs, suggesting that ADAM10 specifically cleaves NLG1 but not NLG2. These data suggest

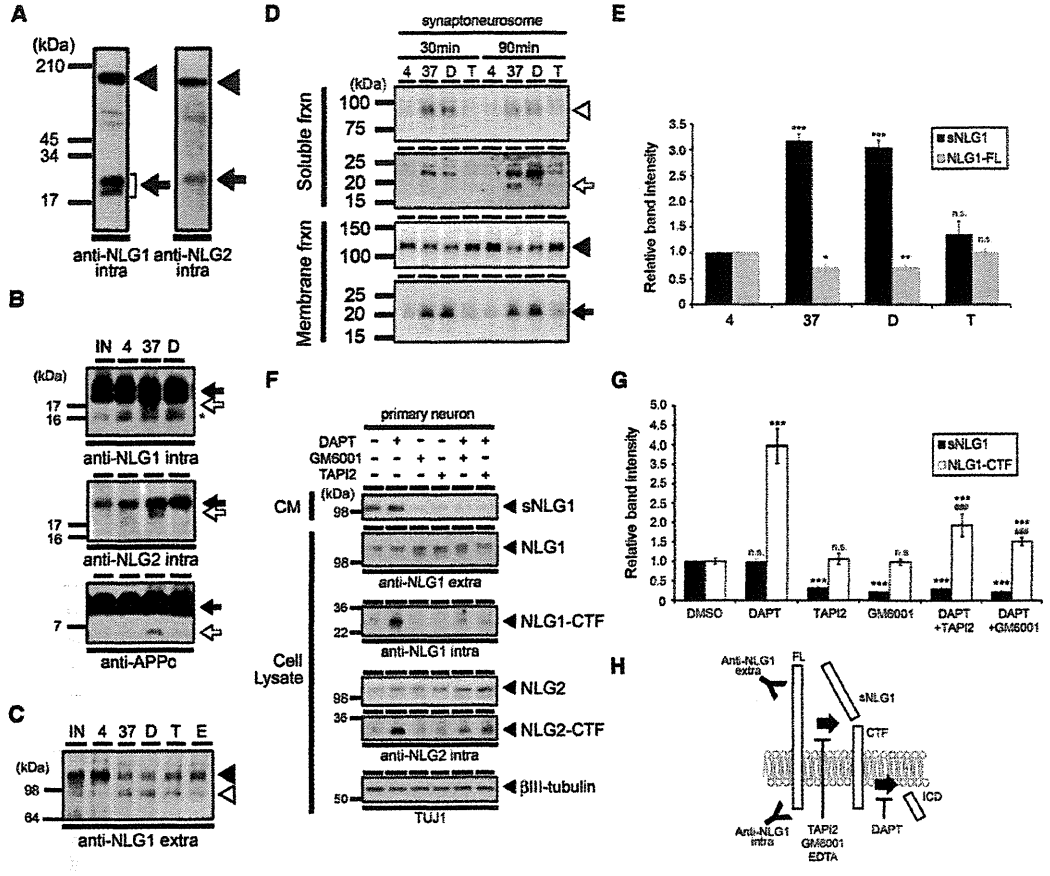

Figure 1. Proteolytic Processing of Endogenous NLGs in Rat Brains

(A) Immunoblot analysis of membrane fraction from adult rat cortex using an antibody against the intracellular domain of NLGs. Molecular weight was indicated on the left.

(B) Processing of NLG-CTFs in the cell-free assay using membrane fractions from adult rat cortex. Used antibodies are indicated below the panel. Arrows, open arrows, and asterisks represent CTFs, ICDs, and nonspecific bands, respectively. IN, input; 4, incubation at 4°C; 37, incubation at 37°C; D, incubation at 37°C with DAPT.

(C) Shedding of NLG1-FL in the cell-free assay. Arrowhead and an open arrowhead denote NLG1-FL and secreted NLG1, respectively. E, samples incubated with EDTA; T, samples incubated with TAPI2.

(D) Incubation of synaptoneurosome fraction from adult mouse brain. Open arrowhead, open arrow, arrowhead, and arrow denote sNLG1, NLG1-ICD, NLG1-FL, and NLG1-CTF, respectively. 4, incubation at 4°C; 37, incubation at 37°C; D, incubation at 37°C with DAPT; T, incubation at 37°C with TAPI2.

(E) Densitometric analysis of sNLG1 (black bar) and NLG1-FL (gray bar) in (D) (n = 3, mean ± SEM; $^{*}p < 0.05$; $^{**}p < 0.01$; $^{***}p < 0.001$ versus 4 degrees by Student's t test).

(F) Primary neurons from E16 mouse at DIV10 were treated with indicated inhibitors for 48 hr. Conditioned medium (CM) and cell lysates were analyzed by immunoblot analysis with antibodies indicated below the panels.

(G) Densitometric analysis of sNLG1 (black bar) and NLG1-ICD (white bar) in (F) (n = 4–6, mean ± SEM; $^{***}p < 0.001$ versus DMSO; $^{###}p < 0.001$ versus DAPT by Student's t test).

(H) Schematic depiction of NLG processing.

that ADAM10 and γ-secretase are responsible for the proteolytic processing of NLG1 in transfected fibroblasts.

To further examine the role of ADAM10 in the processing of endogenous NLG1, we treated rat primary neurons obtained from E18 pups with INCB3619, a known ADAM10/17 inhibitor (Witters et al., 2008). INCB3619 abolished the secretion of sNLG1 in a similar manner to that of sAPPα, the latter being generated by ADAM10 (IC_{50}: 1.6 μM) (Figures 3A and 3C). In contrast, treatment with INCB3420, a derivative of INCB3619 that harbors a moderate ADAM10/17 inhibitory activity but potently inhibits matrix metalloproteases (MMPs) (i.e., MMP2, MMP9, MMP12, and MMP15) (Zhou et al., 2006), decreased the NLG1 cleavage only at high concentrations (IC_{50}: >10 μM) (Figures 3B and 3C). In addition, INCB3420 did not affect the sNLG1 production by incubation of synaptoneurosome fraction of rat adult brain (Figure S2A). Moreover, other MMP-specific inhibitors with different chemical structures (MMP2, MMP3, MMP9, and MMP13 inhibitors) did not affect the sNLG1

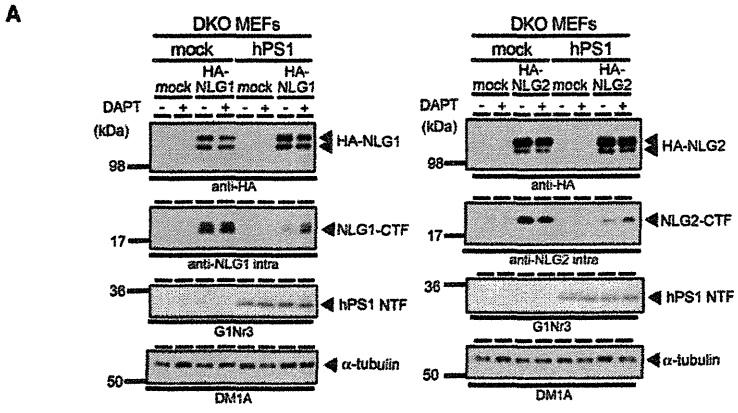

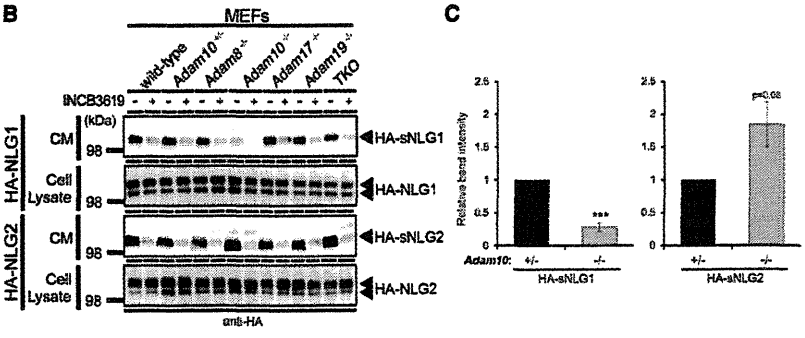

Figure 2. Proteolytic Processing of NLG1 in Presenilin or ADAM Knockout Cells

(A and B) Immunoblot analysis of HA-NLG1 or HA-NLG2 overexpressed in MEFs obtained from PS1/PS2 DKO (A) or ADAM KO (B) mice. Twenty-four hours after treatment of indicated compounds (i.e., 10 μM of DAPT in A, 10 μM of INCB3619 in B), CM and cell lysates were analyzed using antibodies indicated below the panels. Genotypes of ADAM knockout cells were indicated above the lanes. TKO denotes cells derived from *Adam9*$^{-/-}$; *Adam12*$^{-/-}$;*Adam15*$^{-/-}$ triple knockout mice.

(C) Densitometric analysis of HA-sNLG1 and HA-sNLG2 in *Adam10*$^{+/-}$ and *Adam10*$^{-/-}$ cells (B) (n = 4, mean ± SEM; ***p < 0.001 versus heterozygous cells [black bar] by Student's t test).

production or decreased only at high concentrations from rat primary neurons, supporting the specific role of ADAM proteases in NLG1 shedding in primary neurons (Figures 3B and 3D). We then examined the effect of genetic ablation of *Adam10* in mouse neuroblastoma neuro2a cells (Figures 3E and 3F) as well as in primary neurons from P1 *Adam10*$^{flox/flox}$ mice (Yoda et al., 2011) (Figures 3G and 3H) by siRNA transfection and overexpression of Cre recombinase, respectively. Inhibition of NLG1 shedding, along with impairment of sAPPα generation as previously described (Jorissen et al., 2010; Kuhn et al., 2010), and accumulation of NLG1-FL were observed both in *Adam10* knockdown neuro2a cells and *Adam10* knockout neurons. Moreover, overexpression of ADAM10 in mouse primary neurons increased the production of sNLG1 (Figure S2B). Lastly, to demonstrate the physiological significance of ADAM10 in NLG1 processing in vivo, we incubated the brain microsome from postnatal day (P) 18 neuron-specific conditional ADAM10 knockout mice (*Adam10*$^{flox/flox}$; *CamKII-Cre*) (Figure 3I). Notably, the levels of NLG1-FL were increased in the microsome fractions from brains of *Adam10* conditional knockout mice, whereas sNLG1 production was significantly decreased (Figures 3J and 3K). Taken together, we concluded that the major physiological sheddase of NLG1 in brain is ADAM10.

We next examined the proteolytic processing of NLG1 at the ectodomain in more detail. According to the molecular weight of the CTF, the stalk region of NLG1 is predicted as the candidate cleavage site for shedding. To obtain further precise information on the location and characteristics of the cleavage site, we analyzed mutant forms of NLG1 overexpressed in COS-1 cells (Figure 4A). Recombinant NLG1-FL was sequentially cleaved similarly to the endogenous NLG1-FL in primary neurons, whereas NLG1-ICD was not observed (Figures 4B and 4C). To identify the extracellular cleavage site of NLG1, we have systematically generated a series of alanine substitutions around the juxtamembrane stalk region, at sites consistent with the molecular weight of sNLG1 and NLG1-CTF: K^{674}QDD/AAAA, P^{678}KQQ/AAAA, P^{682}SPF/AAAA, S^{686}VDQ/AAAA, R^{690}DYS/AAAA, and T^{694}E/AA (Figure 4A). Among these mutants, generation of sNLG1 was significantly decreased in the PKQQ/AAAA mutant, whereas the level of mutant FL protein was increased (Figures 4D and 4E). The observation that overexpressed PKQQ/AAAA mutant NLG1 accumulated at dendritic spines in rat primary neurons similarly to wild-type (WT) NLG1 and showed spinogenic effects supported the view that introduction of PKQQ/AAAA mutation did not affect the trafficking of NLG1 (see Figure 8C). In contrast, alanine substitutions at regions proximal to the membrane caused an augmentation of NLG1 shedding. Intriguingly, the levels of sNLG1 were significantly increased in the PSPF/AAAA and SVDQ/AAAA mutants, whereas the corresponding FL proteins were decreased, suggesting that the region from Pro^{682} to Gln^{689} negatively regulates the NLG1 shedding. These data suggest that the region between Pro^{678} to Gln^{681} is critical for the sNLG1 production.

We then overexpressed NLG1-ΔE, a recombinant polypeptide corresponding to NLG-CTF starting from residue Val^{682} fused with a signal peptide (Figure 4A). The levels of NLG1-ΔE were increased by DAPT treatment, indicating that NLG1-ΔE was processed by γ-secretase (Figure 4F). However, NLG1-ICD was again undetectable in lysates of transfected cells. Indeed, recombinant NLG1-ICD, which corresponds to the predicted γ-secretase product starting at an intramembranous residue Val^{717}, was detected only after proteasome inhibitor treatment (Figure 4G), suggesting that NLG1-ICD is highly labile to proteasomal degradation. In fact, the immunostaining of NLG1-ICD

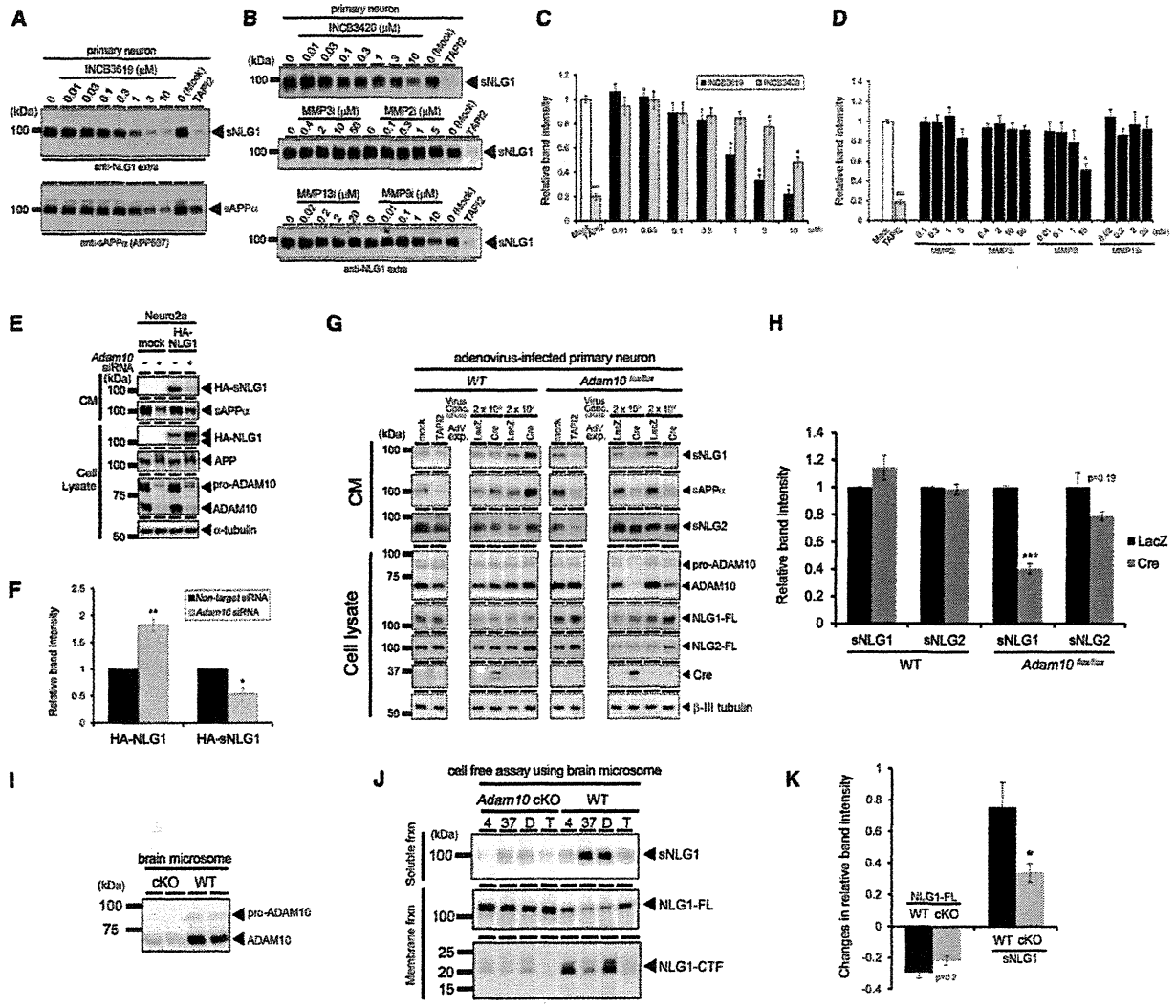

Figure 3. Pharmacological and Genetic Analyses of NLG1 Shedding in Neurons

(A and B) Immunoblot analysis of CM of rat primary neurons obtained from E17–E18 pups treated with ADAM (A) or MMP (B) inhibitors at DIV4. CM was collected at DIV6. Used compounds and concentration are shown above the lanes.

(C and D) Densitometric analysis of sNLG1 from neurons treated with ADAM (C) or MMP (D) inhibitors (n = 4–8, mean ± SEM; $^{\#\#\#}p < 0.001$ versus mock by Student's t test; $^{*}p < 0.05$ versus mock by one-way ANOVA followed by Dunnett's post test).

(E) Immunoblot analysis of overexpressed HA-NLG1 in neuro2a cells cotransfected with siRNA duplex for nontarget or *Adam10*. CM and cell lysates were analyzed by immunoblotting using anti-HA for HA-NLG1, APP597 for endogenous APP, and anti-ADAM10 and DM1A for α-tubulin.

(F) Densitometric analysis of HA-NLG1 and HA-sNLG1 in (E) (n = 4, mean ± SEM; $^{*}p < 0.05$, $^{**}p < 0.01$ versus nontarget siRNA by Student's t test).

(G) Immunoblot analysis of mouse primary neurons infected with recombinant adenoviruses. Neurons were obtained from wild-type or *Adam10*$^{flox/flox}$ mouse at P1 and infected at DIV4 and replaced with fresh medium at DIV6. Samples were obtained at DIV8 and subjected to immunoblot analysis.

(H) Densitometric analysis of sNLG1 and sNLG2 in (G) (n = 3–6, mean ± SEM; $^{***}p < 0.001$ versus lacZ-infected cells by Student's t test).

(I) Immunoblot analysis of brain microsomes obtained from *Adam10*$^{flox/flox}$; *CamKII-Cre* (cKO) and *Adam10*$^{flox/flox}$ (WT) mice at P18.

(J) Cell-free assay of brain microsomes from cKO and WT mice. After incubation, samples were centrifuged to separate soluble and membrane fractions and then subjected to immunoblot analysis.

(K) Relative changes in the levels of NLG1-FL and sNLG1 in (J) compared with that at 4 degrees (n = 3, mean ± SEM; $^{*}p < 0.05$ versus WT by Student's t test).

was relatively weak and predominantly detected in neuronal nuclei and somata, whereas NLG1-FL, as well as the other mutants, was localized to the somatodendritic compartments in transfected primary neurons (Figure S3). We further examined the significance of the PDZ-binding motif located at the C terminus of NLG1 and found that deletion of this motif did not impact on the shedding as well as the γ-secretase-mediated cleavage (Figures 4A, 4B, 4C, and 4F). Collectively, these data

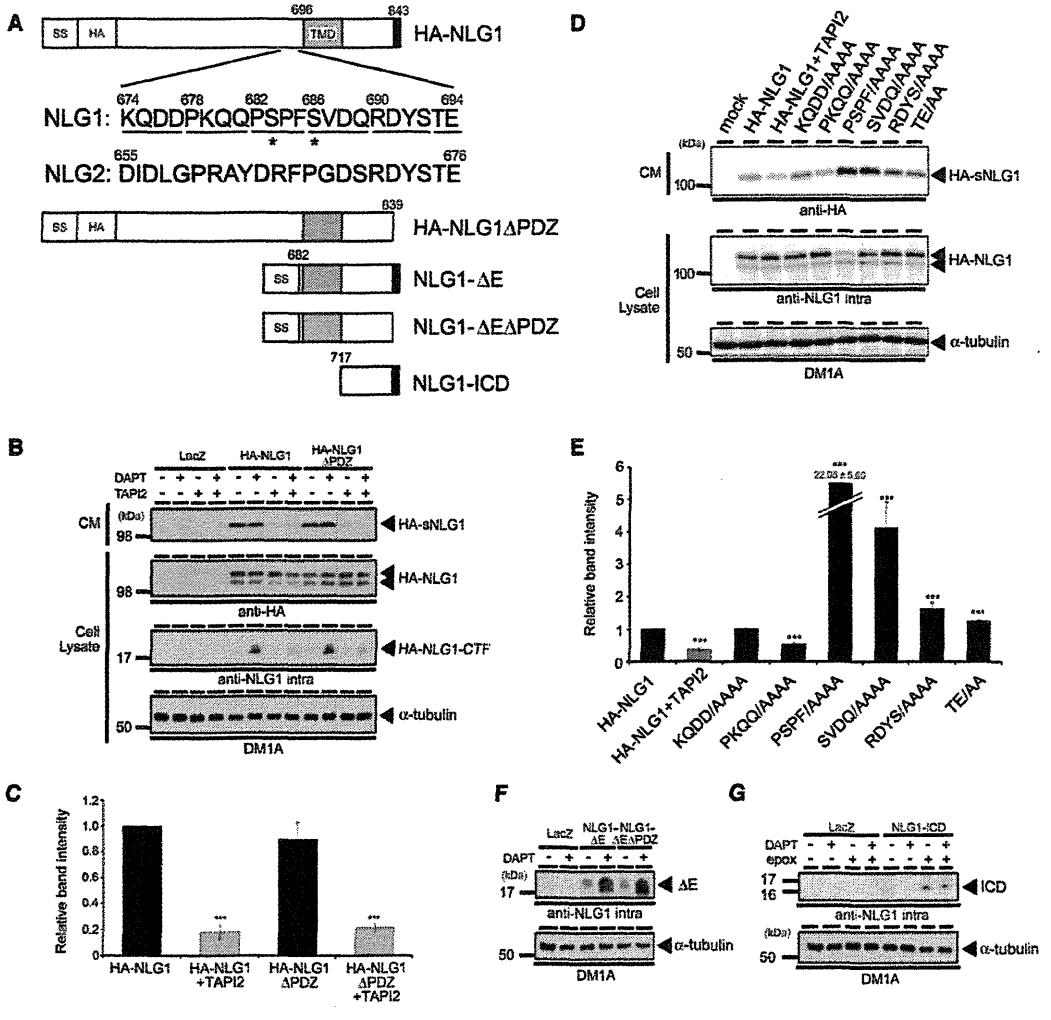

Figure 4. Proteolytic Processing of Mutant Forms of NLG1 at the Predicted Cleavage Site in COS-1 Cells

(A) Schematic depiction of mutant NLG1 constructs used in this study. Numbers represent corresponding amino acid residues in mouse NLG1. Transmembrane and PDZ-binding domains are indicated as gray and black boxes, respectively. Boxes with SS and HA represent signal sequence and inserted HA tag, respectively. Primary amino acid sequences of the stalk region of NLG1 and NLG2 are shown by single letter code. Locations of alanine substitution mutations in NLG1 were indicated by underbar. Asterisks represent O-glycosylation sites in the stalk region of NLG1.

(B–G) Immunoblot analysis of CM as well as lysates of COS cells expressing NLG1ΔPDZ (B), NLG1 with amino acid substitutions (D), NLG1-ΔE (F), or NLG1-ICD (G) treated with indicated compounds. Note that NLG1-ICD was detected only in epoxomicin (epox)-treated COS cells. Densitometric analysis of secreted HA-sNLG1 standardized by HA-NLG1 expression of lysates in (E) and (D) were shown in (C) and (E), respectively ($n = 3$, mean ± SEM; ***$p < 0.001$ versus HA-NLG1 by Student's t test).

support the notion that NLG1 is sequentially cleaved by ADAM10 and γ-secretase to release sNLG1 and a highly labile NLG1-ICD.

Neuronal Activity and Ligand Binding Upregulate NLG1 Processing

It has been shown that some γ-secretase substrates (e.g., APP, N-cadherin, and EphA4) undergo cleavage in an activity-dependent manner in neurons (Kamenetz et al., 2003; Marambaud et al., 2003; Reiss et al., 2005; Inoue et al., 2009). To investigate the effect of synaptic activity on NLG1 processing, we treated rat primary neuronal culture at day in vitro (DIV) 11 with a set of compounds. Fifteen minute treatments with glutamate or NMDA significantly increased the sNLG1 level in the conditioned media, which was abolished by addition of NMDA receptor antagonists (i.e., D-AP5 and MK-801) (Figures 5A and 5B). Intriguingly, pretreatment with MK-801 (Figures 5C and 5D), an open-channel blocker of NMDA receptor (Huettner and Bean, 1988), completely inhibited the NLG1 shedding induced by glutamate, suggesting that the physiological activation of functional NMDA receptors is sufficient for the generation of sNLG1 at the glutamatergic synapses. To examine whether the shedding regulates the cell surface level of NLG1, we performed